UNIVERSITY OF CALIFORNIA, MERCED

Surface Complexation and Reactivity of Kaolinite and Gibbsite with Cadmium: A multi-method approach

A Thesis submitted in partial satisfaction of the requirements

for the degree of Master of Science

in

Environmental Systems

by

Molly A. Small

Committee in charge:

Professor Peggy A. O'Day, Chair

Professor Teamrat A. Ghezzehei

Professor Samuel J. Traina

The Thesis of Molly Ann Small is approved, and it is acceptable in quality and form for publication on microfilm and electronically:

Teamrat A. Ghezzehei

Samuel J. Traina

Chair, Peggy A. O'Day

THESIS ABSTRACT

Determination of energetically favorable surface complexes that form at the mineral-solution interface is important for understanding the surface reactivity of common minerals such as kaolinite and gibbsite and the behavior of toxic pollutants such as Cd^{2+}. In this study, experimental Cd L_{III} X-ray Absorption Near-Edge Structure (XANES) was combined with periodic density functional theory (DFT), theoretical XANES calculations of the Cd L_{III} edge, and surface complexation modeling to characterize Cd^{2+} complexes sorbed to surfaces. Cd L_{III} spectra were collected for Cd^{2+} reference compounds, aqueous solutions, and sorption samples. Linear combination fitting of sorption sample XANES spectra was performed with known compounds and a sorption sample spectrum at low Cd surface coverage (IS-Kaol) that was interpreted to represent a mononuclear inner-sphere complex. With increasing surface coverage, spectra showed a systematic decrease in the fraction of IS-Kaol reference, indicating that as surface coverage increases, the proportion of bidentate complexes decreases. In linear combination fits, a component interpreted as a dimeric component ($CdAlO_4$(s) or $Cd(OH)_2$) increased with surface coverage, suggesting that dimerization or surface reformation may be occurring when surface coverage is high. A postulated set of Cd^{2+} surface reactions on the (100) face of kaolinite and gibbsite were compiled as constrained by DFT calculations and Cd L_{III} XANES. The Charge Distribution MUlti-SIte Complexation (CD-MUSIC) model was used in PhreePlot with this constrained set of reactions and used to derive complexation constants. Sorption on gibbsite was fit with a mononuclear bidentate reaction at low surface coverage (1 Cd/300 nm^2), and with bidentate and dimer reactions at high coverage (1 Cd/3 nm^2). Sorption on kaolinite was

fit with a bidentate reaction at low surface coverage (1 Cd/150 nm^2), and with bidentate, monodentate, and outer-sphere reactions at high surface coverage (1 Cd/1.5 nm^2). The results indicate that mononuclear inner-sphere complexes form first on both kaolinite and gibbsite. With increased surface coverage, dimer complexes form on gibbsite, and outer-sphere complexes form on kaolinite, which is consistent with results from linear combination fits.

ACKNOWLEDGEMENTS

This research was funded by the National Science Foundation, CHE-1213407, "Collaborative Research: Quantifying the Reactive Surface Area of Environmental Solids".

First, I would like to thank my committee for their support and investment of time and energy in this project.

Thank you to Liying Zhao at Sierra Nevada Research Institute Environmental Analytical Laboratory, UC Merced; Mike Dunlap at Imaging & Microscopy Facility, UC Merced; Stanford Synchrotron Radiation Lightsource at SLAC; and Suzanne Estok at Pennsylvania State University for FESEM pictures.

Thank you to Maritza Flores-Marquez for assistance with experiments and data collection.

Thank you especially to my adviser, Peggy O'Day, and lab mates Masakazu Kanematsu, Rasesh Pokharel, Estela Reinoso-Maset, and Elisabeth Neubauer for continued laboratory, computational, and moral support.

My husband, Brandon Small, deserves special commendation for seeing me through this process. Thank you also to my parents, Mary and Mark Thompson, and my sister Jillian Wilson.

TABLE OF CONTENTS

LIST OF TABLES

LIST OF FIGURES

Chapter 1: An Overview

The fraction of a mineral that participates in surface reactions with the environment is known as the reactive surface area. This is distinctly different from the physical surface area, which is simply a geometric measure. Not only does the reactive surface area differ from the geometric surface area, but the fraction is also different for different minerals. Knowing the reactive surface area and the pertinent reactive sites and complexes is important for interpreting how aqueous ions will interact with natural surfaces.

In order to understand reactive surface area, sorption experiments, molecular dynamics calculations, spectroscopy, and surface complexation modeling were employed. We began by performing Cd^{2+} sorption experiments on kaolinite and gibbsite to calculate uptake curves (see Chapter 3 for details on sorption experiments). Experiments were performed over a range of solid and solution variables, including surface coverage, ionic strength, pH, and reaction time. Solid, reacted mineral phases were separated and analyzed by X-ray Absorption Spectroscopy (XAS) at the Stanford Synchrotron Radiation Lightsource. X-ray Absorption Near-Edge Structure (XANES), which focuses on the spectral edge region, was used to analyze the Cd L_{III} edge. XANES was also collected on a variety of Cd^{2+} reference compounds, each showing unique spectral features. Such features were used to explain the stoichiometry of surface complexes and deconvolve the proportions of each species.

Spectra of reference compounds were used as standards in linear combination fits to describe the proportion and nature of complexes forming at the mineral surfaces. From

the trends of these fits, we were able to determine which types of complexes are likely to form over a range of surface coverage.

Heath Watts and James Kubicki, our collaborators at The Pennsylvania State University, use periodic density functional theory (DFT) calculations to determine adsorption energies and molecular structures of Cd^{2+} on kaolinite and gibbsite using the Vienna Ab-initio Simulation Package (VASP) (Kresse and Furthmüller, 1996; Kresse et al., 1994; Kresse and Hafner, 1993, 1994). Clusters were extracted from these energy-minimized models and used in the calculation of theoretical XANES. Niranjan Govind, a research scientist at Pacific Northwest National Laboratory, performed the theoretical XANES calculations with NWChem (Lopata et al., 2012; Valiev et al., 2010; Van Kuiken et al., 2013). The theoretical and experimental XANES were compared to determine whether the complex calculated with periodic density theory was similar to the complexes present on laboratory samples.

The adsorption energies and bond-distances calculated by Watts and Kubicki were used to determine which surface complexes were more probable. This information, along with that obtained from linear combination fits and theoretical XANES, was compiled to constrain a surface complexation model of Cd^{2+} sorption on kaolinite and gibbsite. The Charge Distribution MUlti-SIte Complexation model (CD-MUSIC) was chosen for its ability to model multiple surfaces and its flexibility in incorporating data from multiple sources. Only those reactions that were simulated and energetically favorable were included in the model. In this way, the model is more of a simulation than

a fitting exercise, creating an iterative, multi-method approach to understanding the surface chemistry of common minerals.

Chapters 2 and 3 are manuscripts in preparation for the submission to journals, and are therefore presented separately.

Chapter 2: Experimental and Theoretical XANES Spectra of Cadmium Surface Complexes

ABSTRACT

Determination of energetically favorable surface complexes that form at the mineral-solution interface is important for understanding the surface reactivity of common minerals such as kaolinite and gibbsite and the behavior of toxic pollutants such as Cd^{2+}. In this study, experimental Cd L_{III} XANES was combined with DFT calculations and theoretical XANES calculations of the Cd L_{III} edge to characterize Cd^{2+} complexes sorbed to surfaces. Energy-minimized surface complexes from DFT calculations were used to calculate XANES spectra with the NWChem computational chemistry program, and compared to experimentally collected spectra. Cadmium L_{III} spectra were collected for Cd^{2+} reference compounds, aqueous solutions, and sorption samples. Cadmium sorption experiments were conducted with kaolinite or gibbsite, Cd^{2+} ($CdCl_2$, from 0.1 mM to 4 mM), and a constant background electrolyte ($CaCl_2$) concentration (~10 and ~100 mM) and equilibrated for 1 or 36 d. A spectrum of Cd^{2+} adsorbed to kaolinite at the lowest surface coverage achieved experimentally (IS-Kaol) had unique spectral features and could not be fit with linear combinations of existing reference spectra. IS-Kaol was interpreted to be unique and used as a reference spectrum for mononuclear inner-sphere complexes. With increasing surface coverage, spectra showed a systematic decrease in the fraction of IS-Kaol in the fit, indicating that as surface coverage increases, the proportion of bidentate, inner-sphere complexes decreases. In linear combination fits, a

component ($CdAlO_4$(s) or $Cd(OH)_2$) also increased with higher surface coverage, suggesting that dimerization may be occurring when surface coverage is high. Kaolinite spectra from experiments with low ionic strength had a larger fraction of the outer-sphere ($CdCl_2$(aq)) component when compared with those of high ionic strength, suggesting an expansion of the electrical double layer.

1. INTRODUCTION

Constraining the stoichiometry of surface complexes and determining the reactive sites on mineral surfaces are important to understanding of the reactive surface area of minerals. Different populations of surface complexes are present as surface loading and solution conditions change. Local bonding environments can be interpreted using X-ray Absorption Spectroscopy (XAS), and verified with periodic Density Functional Theory (DFT) calculations via the Vienna Ab-initio Simulation Package (VASP) (Kresse and Furthmüller, 1996; Kresse et al., 1994; Kresse and Hafner, 1993, 1994) and theoretical X-ray Absorption Near Edge Structure (XANES) calculations. The combination of molecular dynamics, XANES calculations, and experimentally collected spectra is a novel three-pronged approach that can cross-reference trends in surface complexation behavior.

The clay mineral kaolinite ($Al_2Si_2O_5(OH)_4$) and hydroxide mineral gibbsite ($Al(OH)_3$) are commonly used as model minerals for Cd^{2+} and other model cation sorption because of their known crystal structures and absence of cation exchange capacity in their pure form. The sorptive properties of kaolinite (Choi et al., 2006; Crosson et al., 2006; Grafe et al., 2007; Gu and Evans, 2008) and gibbsite (Hiemstra and Van Riemsdijk, 1991; Hiemstra et al., 1999; Kubicki and Apitz, 1998; Weerasooriya et

al., 2000; Weerasooriya et al., 2002) have been thoroughly studied. Kaolinite is a well-defined clay mineral consisting of a tetrahedrally coordinated silica layer and an octahedrally coordinated alumina layer, which form sheets. Kaolinite has no cation exchange capacity, and any cation exchange capacity in natural kaolinites comes from mineral impurity, such as the presence of smectite. Gibbsite is a metal hydroxide mineral, and resembles the octahedrally coordinated alumina layer in kaolinite. Gibbsite, like kaolinite, lacks cation exchange capacity, making it an excellent choice for researching reactive surface area. Hydroxylated sites on kaolinite and gibbsite control sorption to their mineral surfaces, which can be investigated with sorption experiments. Many studies have addressed the stoichiometry and reactivity of surface complexes through surface complexation modeling. Gu and Evans (2008) proposed monodentate reactions on both the basal plane (001) and edges (100) of kaolinite, while Srivastava et al. (2005) made the case for a monodentate metal$(OH)^+$ edge reaction. Bidentate reactions are often proposed, splitting the positive surface charge across multiple sorption sites (Serrano et al., 2009; Srivastava et al., 2005). There is also the possibility for outer-sphere hydrated complexes and the reformation of the mineral surface (Bradl, 2004), neither of which are easily addressed by surface complexation modeling. The (100) surfaces of both kaolinite and gibbsite were considered, due to reactivity over a large pH range. The (001) surface of gibbsite is only reactive at very high pH values, and the (001) surface of kaolinite is reactive only due to isomorphic substitution creating non-pH dependent sites.

The idea that surface reactivity changes as surface coverage increases has been discussed (Brown et al., 1999), suggesting that as sites become occupied nearby sites may be rendered less reactive or even unreactive. Even so, some configurations of surface

complexes may be unfavorable and unlikely, and can be systematically tested using DFT calculations. By placing Cd^{2+} cations on a schematic surface of kaolinite or gibbsite in various configurations, surface complexes can be narrowed down by determining which are most favorable under varying conditions.

Synchrotron X-ray absorption spectroscopy (XAS) has commonly been used to analyze local bonding environments, but it is difficult to interpret reactions occurring at the surface when they are part of a bulk measurement. The Cd L_{III} edge was chosen for investigation due to its sensitivity to the immediate bonding environment, and because the few studies using Cd L_{III} XANES have been examined Cd^{2+} complexation with organic compounds or plant material (Isaure et al., 2006; Jalilehvand et al., 2009; Pickering et al., 1999), and did not use the XANES spectra to interpret inorganic interfacial interactions, such as sorption. Only Siebers et al. (2012) attempted linear combination fitting of Cd L_{III} XANES spectra in soils, but examined the bulk speciation behaviors of Cd^{2+} and not sorption mechanisms. Grafe et al. (2007) used Cd K-edge EXAFS to propose the dimerization of Cd^{2+} surface complexes on the surface of gibbsite, and an outer-sphere complex on kaolinite, but only at one surface loading. Although the Cd K-edge would have been useful for corroborating bond distances and interpreting local structure, collecting Extended X-ray Absorption Fine Structure (EXAFS) spectra would have been difficult at low concentrations that are more environmentally relevant.

To our knowledge, the use of Cd L_{III} XANES with linear combination fitting has not been utilized for the interpretation of mineral surface complexation, and is a promising tool for interpreting all types of mineral surface reactions, including outer-

sphere complexation and surface re-precipitation. The comparison of theoretical XANES calculations and experimental spectra is a novel approach to interpreting surface complexation behavior. By combining DFT simulations, theoretical XANES calculations, and experimental XANES, a model of Cd^{2+} surface complexation behavior on kaolinite and gibbsite across changes in surface coverage and solution conditions may be compiled.

2. EXPERIMENTAL SECTION

2.1 Cadmium reference compounds

2.1.1 Synthesis

Some references were ordered from Sigma Aldrich ($CdCO_3$(s), $CdSO_4$(s), $CdCl_2$(s)), and some were synthesized from the ordered materials (Cd(OH)Cl(s), $Cd(OH)_2$(s), and $CdAlO_4$(s), which will be referred to as Cd/Al(s)) (Table 2.1). The $CdCl_2$(s) reference is the same batch and bottle from which solutions for sorption experiments were made. Cadmium hydroxychloride was synthesized by combining 0.110 g of $Cd(OH)_2$(s) and 0.144 g of $CdCl_2$(s) (1 mole of $Cd(OH)_2$ to 1 mole of $CdCl_2$) with 13.6 ml of CO_2-free DI water (Luo et al., 2011). The resulting slurry was loosely covered and placed in an oven at 30°C. Temperature was gradually raised to 50°C over the course of 5 d.

"Cadmium aluminate" was synthesized by combining 45 ml of 0.01 M $CdCl_2$ solution and 100 ml of 0.01 M $AlCl_3$ solution (both CO_2 free), obtaining a molar ratio of 2.2:1 Al^{3+}/Cd^{2+}. After mixing, pH was raised to 12.4 with a drop-wise addition of ~30 ml

0.1 M NaOH solution (Chen et al., 2006). The solution and visible precipitate were stirred via magnetic bar in a closed container for 24 h. The solution and precipitate were poured into two 250 ml centrifuge bottles and centrifuged at 24,000 RCF for 20 min. References were stored at 4°C and were not more than 1 week old when characterized by X-ray absorption spectroscopy and X-ray diffraction (XRD); an aliquot of the solids were also digested for bulk chemical analysis.

2.1.2 Characterization

X-ray diffractograms were collected on reference compounds $Cd(OH)_2$(s), Cd(OH)Cl(s), and Cd/Al(s) at the Imaging and Microscopy Facility at the University of California, Merced. Powder mounts of solids were prepared on zero-background silica plates. Diffractograms were collected with a PanAnalytical X'Pert PRO diffractometer with an ultra-fast X'Celerator detector from 2°-70° 2θ with step size of 0.002° and count time of 10 s using CoKα radiation.

Cd(OH)Cl(s) and Cd/Al(s) were dried at 60°C for 24 h and digested using Anton Paar multiwave 3000 microwave digester. Remaining supernatants were diluted in 2% HNO_3, and analyzed by ICP-OES for aqueous Cd and Al at the Environmental Analytical Lab. Elemental analyses were normalized to the sample dry weight. Limit of quantitation for Cd^{2+} was calculated to be 14 ppb. Limit of quantitation for Al^{3+} was calculated to be 40 ppb. Above the limit of quantitation, analytical error is $\leq \pm 2\%$.

2.2 Sorption Experiments

Sorption of Cd^{2+} onto kaolinite or gibbsite was achieved over a range of Cd^{2+} concentration, ionic strength, and equilibration times. Full details of sorption experiments

can be found in Chapter 3, Section 3.2. The lowest surface coverage spectrum collected was $1.3 \cdot 10^{-8}$ mol Cd/m^2 , equivalent to a bulk concentration of 27 ppm (27 mg/kg dry weight). Samples exhibited a range of adsorbed Cd^{2+} concentrations: 1 Cd/125 nm^2 to 1 Cd/0.53 nm^2 for kaolinite and 1 Cd/ 25 nm^2 to 1 Cd/0.57 nm^2 for gibbsite (Tables 2.2 and 2.3). The solution ionic strength was 30 mM for most samples; 2 samples were examined at lower ("L", ~10 mM) or higher ("H", ~100 mM) ionic strength. Equilibration time was 24 h if not specified, but some samples were equilibrated for 36 d, which is denoted by 'a'. Thermodynamic equilibrium was calculated with PHREEQC at initial conditions to ensure that aqueous solubility of Cd^{2+} was not exceeded with respect to $Cd(OH)_2(s)$. Total Cd and Al were measured via ICP-OES (see Chapter 3 for procedure). The adsorbed Cd^{2+} concentration was calculated by subtracting the residual concentration in solution from the initial concentration. Al was below detection for all samples mentioned (detection limit = 4 ppb) indicating dissolution of mineral phases was minimal near pH 8.

2.3 X-ray Absorption Spectroscopy

2.3.1 Cd L_{III} XANES Spectra

Cadmium L_{III} spectra were collected at the Stanford Synchrotron Radiation Lightsource (SSRL) on wiggler-magnet beamline 4-3 with a Si(111) double-crystal monochromator and nickel focusing mirror with an energy resolution of 0.35 eV. Energy was calibrated using $CdCl_2(s)$, placing the 1st and 2nd inflection points on the adsorption edge at 3532 and 3558 eV, respectively. All dry references, including $CdCl_2(s)$, were mounted as thin smears on Kapton tape and measured at room temperature with the photoelectric Passivated Implanted Planar Silicon (PIPS) detector (Canberra, model

number PD5000-75-500AB). Spectra of aqueous Cd^{2+} solutions were mounted in Teflon sample holders covered front and back with Kapton tape. Aqueous Cd^{2+} solutions (see Table 2.3) were inserted into the sample holder with a needle and syringe. Samples of Cd^{2+} sorbed on kaolinite and gibbsite (see full details of sorption experiments in section 3.2) were packed into Teflon or aluminum sample cells, sealed with Kapton tape, and placed in the beam. Aqueous Cd^{2+} and sorbed Cd^{2+} spectra were collected using a 4-element SiLi Vortex ME-4 detector (Hitachi High-Tech Science Corporation). The background was subtracted from spectra using linear fits in the pre-edge region (3470-3528 eV) and post-edge (3580-3600 eV) regions using the ATHENA software package (Ravel and Newville, 2005).

2.3.2 Linear Combination Fits

Spectra of Cd^{2+} sorption samples were fit by least-squares linear combinations of reference spectra. Three-point interpolative smoothing of noisy spectra was performed on low concentration samples (~1Cd/25nm^2 and lower) where the ratio of signal to noise was low. Only enough smoothing was performed to mimic the signal-to-noise level in higher concentration spectra (1Cd/10 nm^2 and higher). Spectra were fit initially with all combinations of all reference spectra (n=7) to determine which were the most important. Reference spectra were narrowed down to a set of 5 spectra that fit the unknown spectrum best. Final fits were achieved by fitting the unknown spectrum with all combinations of the reference subset with 2 or 3 spectral components in the energy range 3530 to 3568 eV. The weights of the components were not forced to equal 1, energy was not varied, and the χ^2 value was used as a measure of goodness-of-fit:

Equation 1 $$\chi_r{}^2 = \sum \frac{(\chi_{exp}(k)k^3 - \chi_{fit}(k)k^3)^2}{P-F}$$

Where k is the photoelectron wavenumber, $\chi_{exp}(k)$ is the experimental spectrum, $\chi_{fit}(k)$ is the fit spectrum, P is the number of data points and F is the number of free variables. Good fits ($\chi^2 < 6 \bullet 10^{-4}$) were achieved with non-unique combinations of spectra in some cases; for these, the fits that best matched the feature at ~3545 eV were selected. The linear combination fits presented were the best achieved, but may not be completely unique. Some dominant components were consistently present in linear combination fits of unknown spectra. These dominant components varied up to 6% as the third spectral component was changed, and so an uncertainty of 6% was used. The 6% error can also account for some linear combination fits that fail to sum to 100%.

2.4 Theoretical DFT Cluster Calculations and XANES Spectra

Molecular models of postulated surface complexes on kaolinite and gibbsite were created and energy-minimized using DFT calculations with the simulation package VASP. Bidentate, monodentate, and outer-sphere complexes were simulated on the (100) face of both kaolinite and gibbsite. Theoretical XANES were simulated using NWChem (Lopata et al., 2012; Valiev et al., 2010; Van Kuiken et al., 2013) on clusters extracted from DFT-minimized structures. Thus far, theoretical XANES spectra have only been simulated for clusters extracted from kaolinite. DFT minimizations XANES spectra were scaled and energy shifted for comparison with the experimental spectra. The theoretical XANES calculations can only report significant results within 15 eV of the adsorption edge, and so only pre-edge features and adsorption features on the rising limb of the peak can be interpreted.

3. RESULTS

3.1 Sorption

Sorption of Cd^{2+} increased with increasing aqueous Cd^{2+} concentration. Comparing kaolinite samples of similar surface coverage, increasing ionic strength decreases the amount of Cd^{2+} adsorbed to the surface. This phenomenon is not present in gibbsite samples of similar surface coverage. Increased equilibration time was correlated with increased Cd^{2+} surface coverage in both kaolinite and gibbsite samples with the same initial Cd^{2+} concentration.

3.2 Analysis of Reference Compounds

Various Cd^{2+} compounds were chosen and analyzed as references to aid in the interpretation of the Cd L_{III} spectra collected on sorption samples (Table 2.1). The compound Cd/Al(s) reference ('cadmium aluminate') had a Cd:Al ratio of 2.2, indicating non-stoichiometric $CdAlO_4$. The corresponding XRD diffractogram (Figure 2.1C) has a high background, indicating that there is a large amorphous portion. The spectrum was best matched by hydrocalumite, $Ca_2Al(OH)_6Cl\cdot 2H_2O$, although there is still a large remainder. XRD diffractograms of Cd(OH)Cl(s) and $Cd(OH)_2$(s) were well described by database references of the pure compounds.

3.3 Cd L_{III} XANES of Reference Compounds

XANES of the known reference compounds exhibit a number of unique absorption features (Figure 2.2), as well as a consistent feature at 3535 eV that is evidence for coordination with nitrogen or oxygen (Pickering et al., 1999). For this set of

compounds, the feature corresponds to coordination with oxygen. $CdCO_3$(s) and $CdSO_4$(s) show the most unique features, but were not similar to sorption spectra. When linear combination fits were attempted with the reference library of pure compounds, acceptable fits were not achieved. In order to fit the XANES sorption sample spectra, additional reference spectra were needed. Reference spectra were considered with Cd in a local bonding environment similar to that postulated for different types of surface complexes, although references were mot chemically identical to surface complexes on the mineral. The Cd^{2+} solution reference, $CdCl_2$(aq), is used as an analog for an outer-sphere surface complex. Cd/Al(s) and $Cd(OH)_2$(s) were used as proxies for dimerization, where Cd-Cd interactions are occurring. From the sorption experiments, the lowest surface coverage kaolinite experiment (1 Cd/125nm^2 kaolinite), IS-Kaol, presented unique spectral features that were not identified in any other Cd spectra (Figure 2.3). Therefore, it was used as a proxy for the inner-sphere monomer Cd^{2+} complex on mineral surfaces in linear combination fits.

Results from DFT calculations below showed that kaolinite surface complexation reactions with Cd^{2+} were more energetically favorable on aluminol sites rather than silanol sites. Therefore, the IS-Kaol reference was used to fit both kaolinite and gibbsite spectra, inferring that inner-sphere complexes will occur predominantly on aluminol sites on kaolinite, and only on aluminol sites on gibbsite.

3.4 Cd L_{III} XANES of Sorption Samples

3.4.1 Cd L_{III} XANES of Gibbsite Sorption Samples

The IS-Kaol spectrum was fit in all gibbsite linear combination fits. The lowest coverage sample G-0.04 (1 Cd/23 nm^2) was fit with 46% IS-Kaol reference spectrum, which was the highest percentage in the gibbsite linear combination fits. Low coverage samples (1 Cd/2.7 nm^2 to 1 Cd/2.4 nm^2) were fit with the same fraction of IS-Kaol reference within error. The spectra from the highest surface coverage sorption samples (~ Cd/0.6 nm^2) showed differences in the fraction of IS-Kaol reference with changes in ionic strength. Cd/Al(s) was a component in all gibbsite spectra, and $Cd(OH)_2$(s) was a component in five out of eight gibbsite spectra, across the range of surface coverage (Table 2.4).

Spectra at similar surface coverage equilibrated for 24 h and 36 d are compared in Figure 2.4. No significant differences were seen between fresh (24 h) and aged (36 d) gibbsite samples with similar surface coverage.

Gibbsite sorption spectra showed changes across order-of-magnitude variations in ionic strength (Figure 2.5). At high ionic strength, there was an 81% dimer component ($Cd(OH)_2$(s) + Cd/Al(s)) versus a 63% dimer component in the low ionic strength sample. Although the surface coverage was the same in both samples, the high ionic strength sample had a 22% IS-Kaol component versus a 40% IS-Kaol component in the comparable low ionic strength spectrum.

As surface coverage is increased on gibbsite (with the same ionic strength and equilibration time), the proportion of IS-Kaol decreased in the spectral fit and the addition of the $Cd(OH)_2$(s) component (Figure 2.6).

3.4.2 Cd L_{III} XANES of Kaolinite Sorption Samples

The IS-Kaol spectrum was fit in all kaolinite linear combination fits, and the $CdCl_2$(aq) spectrum was used in all linear combination fits with the exception of K-0.1, the second-lowest coverage kaolinite sorption sample. With increased surface coverage on kaolinite, there is an increased proportion of $CdCl_2$(aq) and a decreased proportion of IS-Kaol (Table 2.5).

Kaolinite samples K-0.7a (aged) and K-0.4 (fresh) were compared to determine the effects of aging on surface complexes. The component of $Cd(OH)_2$(s), or the Cd-Cd dimer reference, increases by 7% in the aged sample (Figure 2.7).

Two kaolinite samples (K-1.7H, 140 mM ionic strength, and K-1.8L, 24 mM ionic strength) were compared for effects on Cd^{2+} sorption with changes in ionic strength with similar surface coverage (~1 Cd/0.6 nm^2) (Figure 2.8). With decreased ionic strength, an 18% increase in the $CdCl_2$(aq) component, our proxy for outer-sphere complexes, was observed.

Surface coverage differences in kaolinite were compared using K-0.1 (low coverage) and K-1.8 (high coverage) (Figure 2.9). In K-1.8, the proportion of IS-Kaol decreased by 14% in comparison to K-0.1. In the K-1.8 fit, $CdCl_2$(aq) was an important component (48%), and was not fit in the K-0.1 spectrum. The Cd/Al(s) reference described a significant fraction (42%) of the K-0.1 spectrum, but was not fit in K-1.8.

3.5 Theoretical DFT Cluster Calculations and XANES Spectra

3.5.1 DFT Minimizations on Kaolinite

In all cases, DFT minimizations indicated that Cd^{2+} would bond to aluminol sites when the (100) face of kaolinite and gibbsite were considered. A bidentate complex was calculated at a higher energy, 68 kJ/mole (Figure 2.10). On the kaolinite (100) surface, monodentate and outer-sphere complexes are the most energetically favorable, at 0 kJ/mole and 9 kJ/mole respectively (Figures 2.11 and 2.12).

3.5.2 Theoretical XANES Spectra on Kaolinite

Theoretical XANES were simulated on bidentate, monodentate, and outer-sphere clusters on the kaolinite (100) surface from DFT minimizations. Resulting spectra were compared to both high coverage (sample K-1.8) and low coverage (IS-Kaol reference) spectra. Those with the best qualitative correlation are presented in Figures 2.10-2.12. The bidentate simulation (Figure 2.10) showed the best correlation with low-coverage IS-Kaol. The monodentate spectrum was compared to K-1.8 (Figure 2.11), and the simulated outer-sphere spectrum was compared to the $CdCl_2$(aq) reference used in linear combination fits (Figure 2.12). The monodentate and outer-sphere theoretical XANES show similar features, but the bidentate spectrum was distinctly different. The outer-sphere theoretical XANES and $CdCl_2$(aq) reference spectrum show a similar prominent rising edge.

Theoretical spectra compared in Figure 2.13 show different features unique to the stoichiometry of the surface complex. In the derivative plot, the outer-sphere spectrum has an inflection at approximately 3540 eV, followed by the inflections of the monodentate spectrum and bidentate spectrum.

3.5.3 DFT Minimizations on Gibbsite

Bidentate and monodentate reactions are most favorable on the gibbsite (100) surface, at 0 kJ/mole and 6 kJ/mole respectively (Figures 2.14 and 2.15). A dimer complex was also possible, but at a slightly higher energy, 37 kJ/mole. An outer-sphere complex was calculated, but at 157 kJ/mole, it was the least energetically favorable.

4. DISCUSSION

4.1 Linear Combination Fits

No combination of reference compounds could adequately describe the lowest surface coverage sample IS-Kaol and therefore cannot be analogous to binuclear complexes or outer-sphere complexes. No reference could be found or synthesized that likened to a bidentate complex, and so IS-Kaol was used as a reference compound for inner-sphere complexes. There is a distinct difference between the IS-Kaol spectrum at lowest surface coverage and those at higher surface coverage, indicating that Cd^{2+} surface complexes have a unique bonding environment at very low sorption density. Specifically sorbing inner-sphere complexes are likely to occur at low coverage densities when the surface is not "crowded", but we cannot differentiate a bidentate inner-sphere complex from a monodentate inner-sphere complex. Crystalline compounds such as $Cd(OH)_2(s)$ and synthesized Cd/Al(s) represent binuclear complexes because of the close proximity of Cd within the crystal structure. The $CdCl_2(aq)$ reference represents hydrated, outer-sphere complexation of cadmium.

The IS-Kaol spectrum was a component of all linear combination fits, suggesting that it represents the most common type of surface complex, but the proportion decreases with increasing surface coverage. This may be a mononuclear bidentate or monodentate

surface complex based on DFT calculations. The increasing fraction of the $CdCl_2$(aq) component in kaolinite spectra with surface coverage suggests an increasing proportion of outer-sphere complexes.

4.2 Gibbsite Cd L_{III} XANES

All gibbsite spectra had an important IS-Kaol component (34-46%) and Cd/Al(s) component (48-70%). Five out of eight gibbsite spectra were also fit with a minor $Cd(OH)_2$(s) component (9-13%). $Cd(OH)_2$(s) was usually a component in high ionic strength (>100 mM) or aged samples, with the exception of G-1.6. At low surface coverage, solely IS-Kaol and Cd/Al(s) were fit in two spectra. In contrast to the kaolinite fits, $CdCl_2$(aq) was not necessary for fitting. Since gibbsite is a very reactive mineral, particularly the (100) face (Hiemstra et al., 1989a) more mononuclear and binuclear inner-sphere complexes may be forming on the mineral surface compared to kaolinite, and it may not be energetically favorable to form outer-sphere complexes. At high surface coverage, differences between the aged (36 d) and fresh (24 h) spectra could not be identified. At a lower surface coverage, such as between G-0.37 and G-0.41a, $Cd(OH)_2$(s) was required to fit G-0.41a, but not G-0.37 (Table 2.4). This suggests that at even after 24 h of equilibration at high surface coverage, there are already many dimer complexes, and that additional dimers that form during the following 35 d of equilibration are not distinguishable using XANES and linear combination fits.

Dimerization also occurred with increasing ionic strength on gibbsite. For G-1.6H and G-1.6L, gibbsite linear combination fits had a large component of Cd/Al(s)(63% and 70%) which may indicate and increase of Cd-Cd dimers. The increase in the fraction of

Cd/Al(s) is concurrent with a decrease of the IS-Kaol fraction from 40% to 22%, indicating that with increased surface coverage there are more dimer or surface reformation reactions forming.

As surface coverage increased on gibbsite, the proportion of IS-Kaol generally decreases, although there seems to be some dependence on ionic strength and equilibration time. With increased ionic strength (>100 mM) and aging time, there was a lower percentage of inner-sphere complexes. This is consistent with the hypothesis that as surface coverage increases, there will not be enough room on the surface for specific sorption. This results in dimerization ($Cd(OH)_2(s)$ and Cd/Al(s)) and the possible reformation of the gibbsite surface. The distribution of Cd^{2+} cations in surface complexes as calculated from XANES linear combination fits is documented in Table 2.6. Additional gibbsite linear combination fits can be seen in Figures 2.17-2.18.

4.3 Kaolinite Cd L_{III} XANES

Inner-sphere (IS-Kaol), outer-sphere ($CdCl_2(aq)$) and dimers ($Cd(OH)_2(s)$) were important components in the fitting of kaolinite spectra. The IS-Kaol component generally decreased with increasing surface coverage, although its proportion is linked to the ionic strength of the reactant solution. $Cd(OH)_2(s)$ was fit in all but K-0.1 and K-0.3, with the highest proportion in K-0.7a (Table 2.5). Although $Cd(OH)_2(s)$ was important in this aged sample, it was not as prominent in the other aged sample, K-1.9a. The surface coverage for this sample was much higher, and $CdCl_2(aq)$ may be overwhelming the $Cd(OH)_2(s)$ component. $CdCl_2(aq)$ was an important part of the kaolinite linear combination fits, with a contribution between 24 and 55%. Generally, the fraction of

$CdCl_2$(aq) increased with increasing surface coverage, although there was a marked increase in the low ionic strength sample, K-1.8L. $CdCl_2$(aq) was fit in all kaolinite spectra except K-0.1, a low surface coverage sample. The Cd/Al(s) spectrum was a component in only the low surface-coverage kaolinite fits, which may suggest that initial sorption of Cd^{2+} cations occurs on the aluminol sites of kaolinite.

When comparing spectra from aged and fresh kaolinite sorption samples, it is important to note that these two samples began with the same initial Cd^{2+} concentration, and that surface coverage increased by 62% over the 35 d of additional equilibration time. In the linear combination fits, the $Cd(OH)_2$(s) component increased by 7% in the aged spectrum. Overall, the proportions of surface complexes were similar, but there was a slight increase in the $Cd(OH)_2$(s) (dimer) fraction.

Two kaolinite samples (K-1.7H and K-1.8L) were compared for effects on Cd^{2+} sorption with changes in ionic strength with similar surface coverage. With decreased ionic strength, the $CdCl_2$(aq) component increased, the proxy for outer-sphere complexes. This could suggest an expansion of the electrostatic double layer (EDL) (Stern, 1924) with decreased ionic strength, resulting in more outer-sphere complexation of Cd^{2+}.

With increased surface coverage on kaolinite, there was a change in the set of fit components. At low surface coverage (1 Cd/23 nm^2), IS-Kaol (inner-sphere complexes) and Cd/Al(s) can describe the XANES spectrum. At high surface coverage (1 Cd/0.64 nm^2), the description of complexation is better fit with $Cd(OH)_2$(s) (dimer) and $CdCl_2$(aq) (outer-sphere). The contribution of the Cd/Al(s) reference to the linear combination fits of spectra from low surface coverage kaolinite samples may indicate the specific sorption

of Cd^{2+} to aluminol sites. With increased surface coverage, there was an increased proportion of $CdCl_2(aq)$, indicating that more outer-sphere complexes formed at high surface coverage. The proportion of IS-Kaol decreased with increasing surface coverage, which suggests that as more Cd^{2+} is adsorbed to the mineral surface, there are more non-specific complexes forming, such as the formation of dimers and outer-sphere complexes, which do not directly interact with a surface site. The distribution of Cd^{2+} cations in surface complexes as calculated from XANES linear combination fits is documented in Table 2.7. Additional kaolinite linear combination fits can be seen in Figures 2.19-2.20.

4.4 Theoretical DFT Cluster Calculations and XANES Spectra

The spectrum of IS-Kaol showed good correlation with the theoretical spectra calculated from the bidentate kaolinite (100) model, including two inflections on the rising edge of the spectrum. Theoretical calculations of monodentate and outer-sphere complexes on kaolinite (100) showed reasonable correlation with the K-1.8 spectrum, although further energy-calibration of the theoretical spectra may be necessary.

Differences between the bidentate, monodentate, and outer-sphere kaolinite XANES simulations can be seen in Figure 2.13. The outer-sphere spectrum is the most unique of the three, which is particularly obvious in the derivative plot. This is expected, since the outer-sphere spectrum has a different local-bonding environment than the bidentate and monodentate complexes. It is encouraging that there are discernible differences in the between the simulated spectra.

5. CONCLUSIONS

With increased equilibration time, sorption samples with the same initial Cd^{2+} solution concentration showed increased final surface coverage. Generally, the proportion of inner-sphere complexation, represented by the IS-Kaol reference, decreased with increasing surface coverage in both kaolinite and gibbsite linear combination fits. The dimer component, represented by Cd/Al(s) and $Cd(OH)_2$(s) in gibbsite linear combination fits, increased with in high ionic strength and aged samples. In kaolinite linear combination fits, Cd/Al(s) was only fit in two low coverage samples, indicating that inner-sphere complexes on kaolinite have interactions with aluminum, and that aluminol sites may be the primary reactive site on kaolinite. The $CdCl_2$(aq) spectrum was only fit in kaolinite samples, and its proportion increases with increasing surface coverage, with the exception of K-1.8L, which was equilibrated in a low ionic strength solution (24 mM). When compared to K-1.7H (ionic strength of 140 mM) there was an increase in the $CdCl_2$(aq) component, indicating that at low ionic strength the EDL expands and there was an increase in outer-sphere complexation. All complexes modeled with DFT simulations on the (100) surface of both kaolinite and gibbsite bonded to aluminol sites. The XANES simulation of the bidentate DFT minimization showed the most similarity to the IS-Kaol "low-coverage" reference, and the outer-sphere simulation showed similarities to the $CdCl_2$(aq) reference spectrum. There are observable differences between complexes in the theoretical XANES simulations.

6. TABLES

TABLE 2.1. Cd^{2+} reference solids and solutions

Standards	XANES	XRD	Source	Concentrations
$CdCl_2$(s)	Yes	No	Sigma Aldrich 99.99% pure	
$CdCl_2$ (aq)	Yes	No	Sigma Aldrich 99.99% pure	4 mM $CdCl_2$ in 75 mM $CaCl_2$
$CdCl_2$ (aq) Low Ionic Strength	Yes	No	Sigma Aldrich 99.99% pure	4 mM $CdCl_2$ in 0.75 mM $CaCl_2$
$CdSO_4$(s)	Yes	No	Sigma Aldrich 99.99% pure	
Cd(OH)Cl(s)	Yes	Yes	Lab precipitate	
$CdCO_3$(s)	Yes	No	Sigma Aldrich 99.99% pure	
Cd/Al(s)	Yes	Yes	Lab precipitate	0.13 mM Cd, 0.055 mM Al ± 1.9% 2.4Cd:1Al ratio in solid
$Cd(OH)_2$(s)	Yes	Yes	Lab precipitate	

TABLE 2.2. Experimental conditions for gibbsite sorption samples

Exp #	Initial Cd^{2+} (mM)	Initial Ca^{2+} (mM)	Initial Cl^- (mM)	I.S. (mM)	Min mass (g)	Soln Vol (ml)	Equil time	Equil pH	Surface coverage (1 Cd/nm^2)	Surface coverage (µmol/m^2)
G-0.04	0.1	9.9	20	30	0.60	10.0	24 h	8.5	23	0.072
G-0.37	1.0	9.0	20	30	0.60	10.2	24 h	8.0	2.7	0.62
[a]G-0.41a	0.8	9.2	20	30	0.60	12.5	1 mo	7.8	2.4	0.68
G-0.42H	0.8	110	220	330	0.59	12.4	24 h	7.9	2.4	0.70
G-1.6L	4.0	0.6	9.0	14	0.49	12.7	24 h	7.8	0.64	2.6
G-1.6	4.0	6.0	20	30	0.59	12.7	24 h	7.9	0.64	2.6
G-1.6H	4.0	44	96	140	0.59	12.6	24 h	7.9	0.64	2.6
G-1.9a	4.0	6.0	20	30	0.59	12.8	1 mo	7.7	0.57	2.9

[a]'a' denotes aged samples, or those with reaction times of 36 d. 'H' represents high ionic strength (>100 mM), and 'L' represents low ionic strength (<30 mM).

TABLE 2.3. Experimental conditions for kaolinite sorption samples

Exp#	Initial Cd^{2+} (mM)	Initial Ca^{2+} (mM)	Initial Cl^- (mM)	I.S. (mM)	Min mass (g)	Soln Vol (ml)	Reaction time	Final pH	Surface coverage (1 Cd/nm^2)	Surface coverage (µmol/m^2)
IS-Kaol	0.01	10	20	30	0.39	10.0	24 h	8.4	125	0.013
K-0.1	0.1	9.9	20	30	0.40	9.9	24 h	8.6	11	0.14
K-0.3	1.0	9.0	20	30	0.39	9.7	24 h	7.8	2.9	0.57
K-0.4	0.8	9.2	20	30	0.39	12.1	24 h	8.0	2.4	0.6
[a]K-0.7a	0.8	9.2	20	30	0.40	13.5	1 mo	8.1	1.5	1.1
K-1.7H	4.0	44	96	140	0.39	12.3	24 h	7.8	0.59	2.8
K-1.8	4.0	6.0	20	30	0.39	12.3	24 h	7.8	0.56	2.9
K-1.8L	4.0	4.0	16	24	0.39	12.6	24 h	7.8	0.54	3.1
K-1.9a	4.0	6.0	20	30	0.39	12.5	1 mo	7.5	0.53	3.2

[a] 'a' denotes aged samples, or those with reaction times of 36 d. 'H' represents high ionic strength (>100 mM), and 'L' represents low ionic strength (<30 mM). IS-Kaol is the lowest coverage kaolinite spectra that could not be fit using linear combination, and was used as a reference for inner-sphere Cd^{2+} complexes.

TABLE 2.4. Results for linear combination fits for Cd/gibbsite

Sample	$Cd(OH)_2$(s) (%)	Cd/Al(s) (%)	IS-Kaol (%)	Total	Reduced χ^2 [a]	Surface coverage (1 Cd/nm^2)
G-0.04		0.53	0.46	0.99	9.8	23
G-0.37		0.57	0.43	1.00	5.9	2.7
G-0.41a	0.12	0.48	0.40	1.00	2.5	2.4
G-0.42H	0.11	0.48	0.43	1.02	4.4	2.4
G-1.6H	0.11	0.7	0.22	1.03	2.8	0.64
G-1.6	0.09	0.59	0.35	1.03	2.8	0.64
G-1.6L		0.63	0.40	1.03	3.5	0.64
G-1.9a	0.13	0.55	0.34	1.02	3.4	0.57

[a] Reduced χ^2 = tabulated number * 10^{-4}

TABLE 2.5. Results for linear combination fits for Cd/kaolinite

Sample	$Cd(OH)_2$(s) (%)	$CdCl_2$ (aq) (%)	Cd/Al(s) (%)	IS-Kaol (%)	total	Reduced χ^2 [a]	Surface coverage (1 Cd/nm^2)
K-0.1			0.42	0.55	0.97	8.4	11
K-0.3		0.24	0.31	0.41	0.96	5.0	2.9
K-0.4	0.19	0.40		0.35	0.94	2.4	2.4
K-0.7a	0.26	0.36		0.32	0.94	3.1	1.5
K-1.7H	0.24	0.27		0.45	0.96	2.6	0.59
K-1.8	0.08	0.48		0.41	0.97	2.4	0.56
K-1.8L	0.15	0.45		0.37	0.97	2.1	0.54
K-1.9a	0.08	0.55		0.31	0.94	2.7	0.53

[a] Reduced χ^2 = tabulated number * 10^{-4}

Table 2.6 Calculated atomic distribution of Cd^{2+} on Gibbsite

Sample	atoms Cd	$Cd(OH)_2(s)$	Cd/Al(s)	IS-Kaol
G-0.04	17.77	0	17.80	17.43
G-0.37	18.71	0	17.83	17.40
G-0.41(1mo)	18.75	16.85	17.75	17.37
G-0.42(HIS)	18.71	16.81	17.75	17.40
G-1.6(HIS)	19.32	16.81	17.92	17.11
G-1.6	19.32	16.73	17.84	17.32
G-1.6(LIS)	19.30	0.00	17.87	17.37
G-1.9a	19.38	16.88	17.81	17.30

Actual value = $10^{\text{table value}}$. Numbers represent the distribution of Cd^{2+} cations in surface complexes according to distributions from linear combination fits.

TABLE 2.7. Calculated atomic distribution of Cd^{2+} on Kaolinite

Samples	Total Cd atoms	$Cd(OH)_2(s)$	$CdCl_2(aq)$	Cd/Al(s)	IS-Kaol
K-0.1	17.78	0	0	17.70	17.52
K-0.3	18.37	0	17.16	17.57	17.39
K-0.4	18.45	17.05	17.38	0	17.32
K-0.7(1mo)	18.66	17.19	17.33	0	17.28
K-1.7(HIS)	19.06	17.16	17.21	0	17.43
K-1.8	19.08	16.68	17.46	0	17.39
K-1.8(LIS)	19.10	16.95	17.43	0	17.34
K-1.9(1mo)	19.12	16.68	17.52	0	17.27

Actual value = $10^{\text{table value}}$. Numbers represent the distribution of Cd^{2+} cations in surface complexes according to distributions from linear combination fits.

7. FIGURES

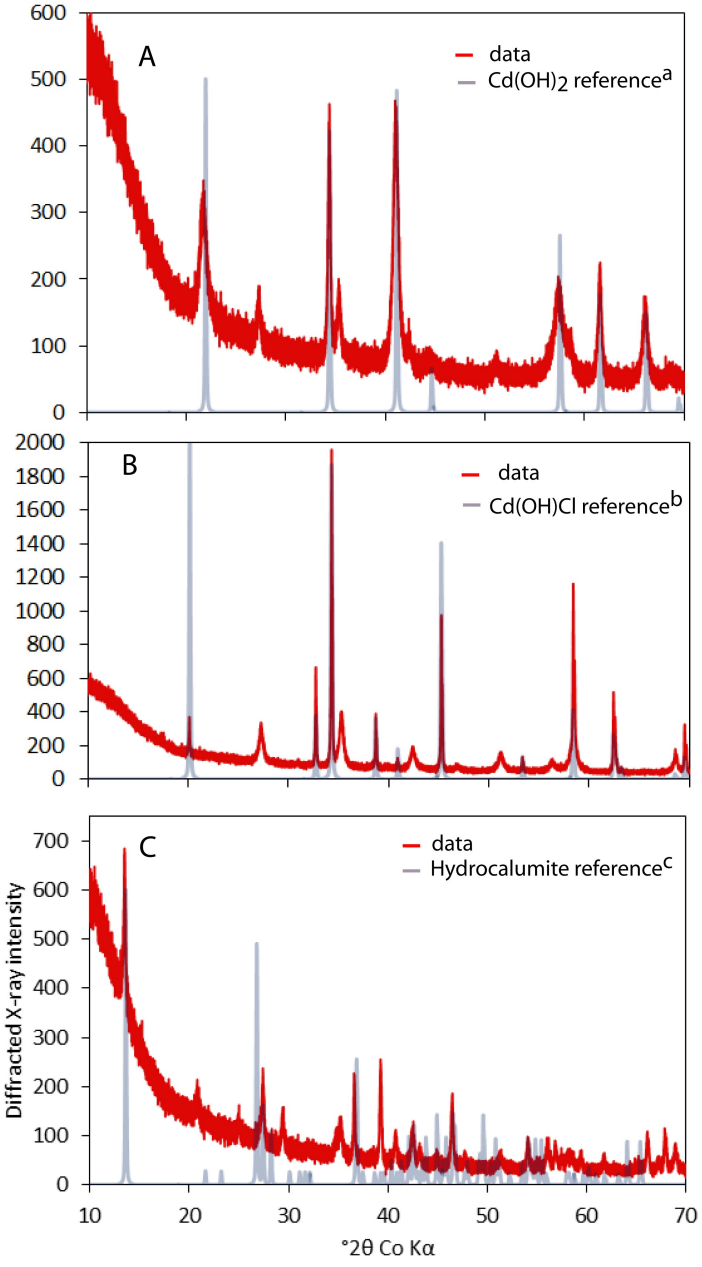

Figure 2.1A-C.

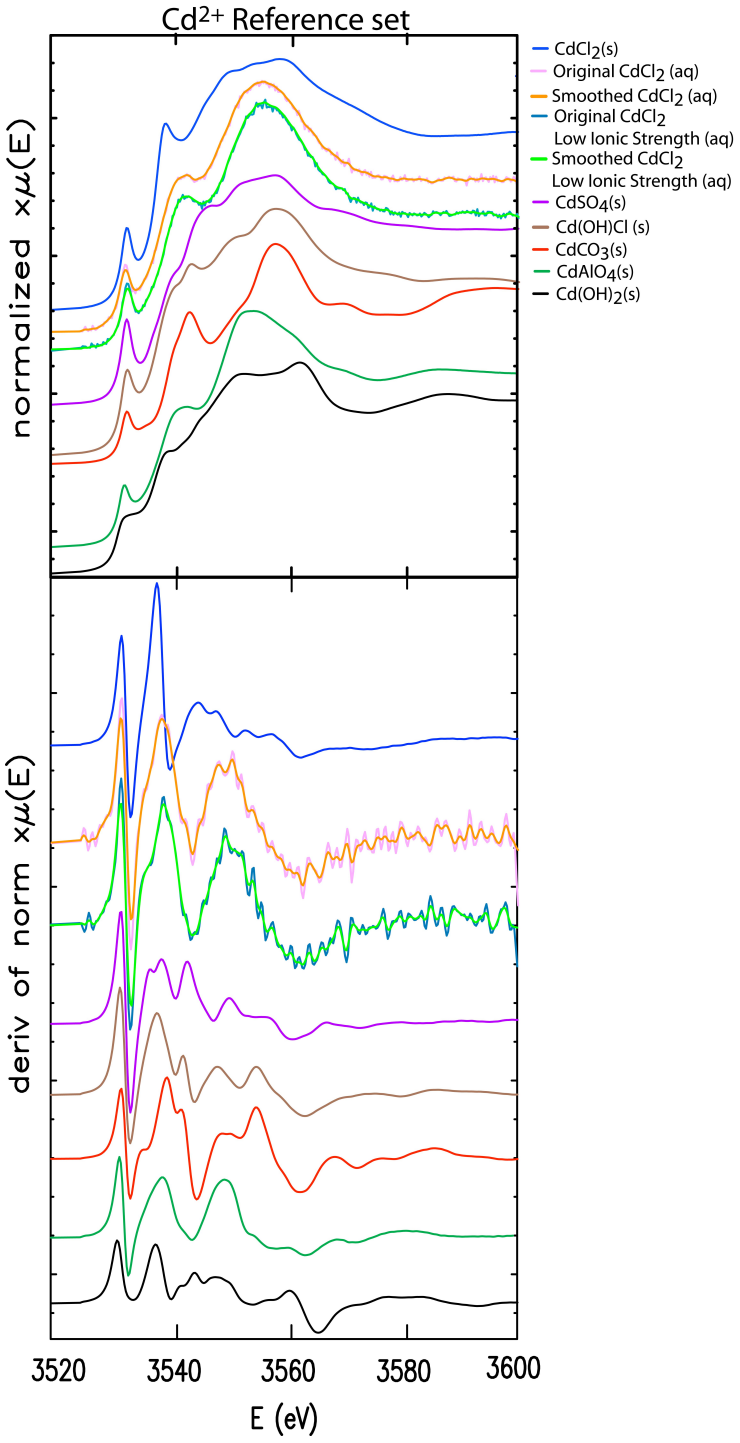
Cd2+ Reference set
normalized xμ(E)
deriv of norm xμ(E)
E (eV)
3520
3540
3560
3580
3600
CdCl2(s)
Original CdCl2 (aq)
Smoothed CdCl2 (aq)
Original CdCl2
Low Ionic Strength (aq)
Smoothed CdCl2
Low Ionic Strength (aq)
CdSO4(s)
Cd(OH)Cl (s)
CdCO3(s)
CdAlO4(s)
Cd(OH)2(s)

Figure 2.2.

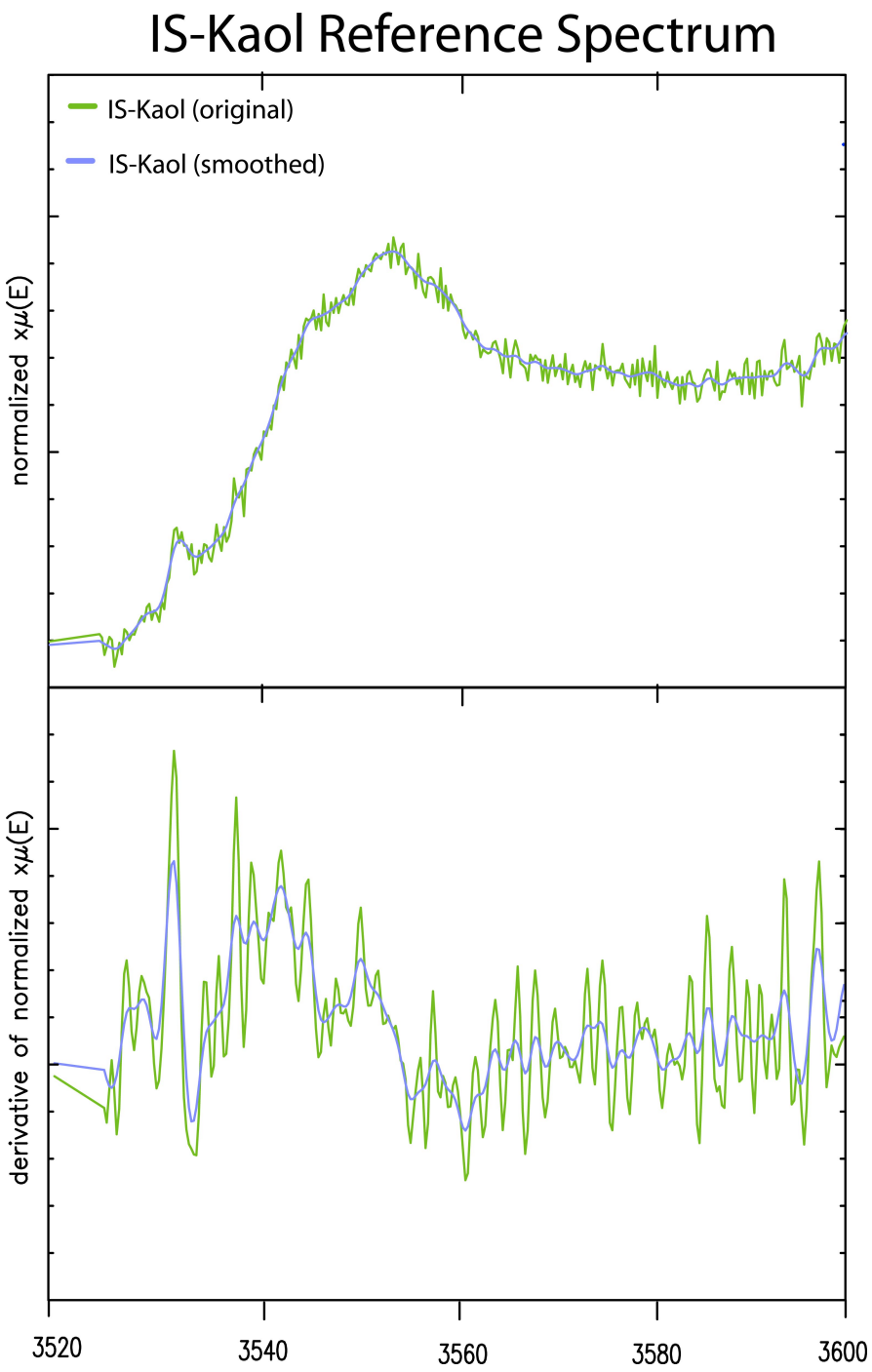
IS-Kaol Reference Spectrum
IS-Kaol (original)
IS-Kaol (smoothed)
normalized xμ(E)
derivative of normalized xμ(E)
3520
3540
3560
3580
3600

Figure

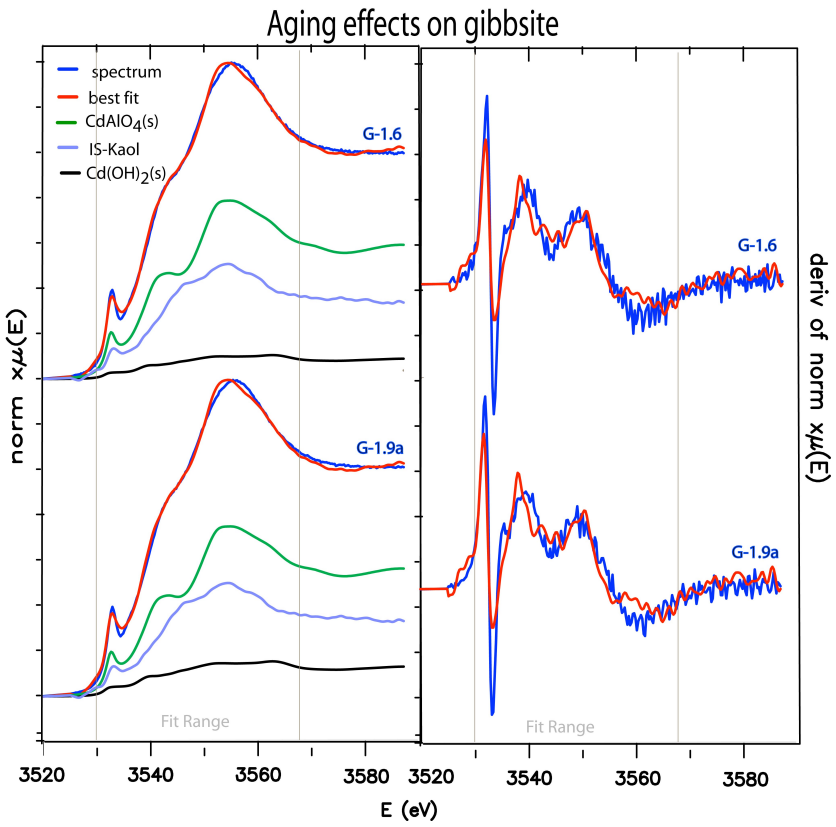

2.3

Figure 2.4

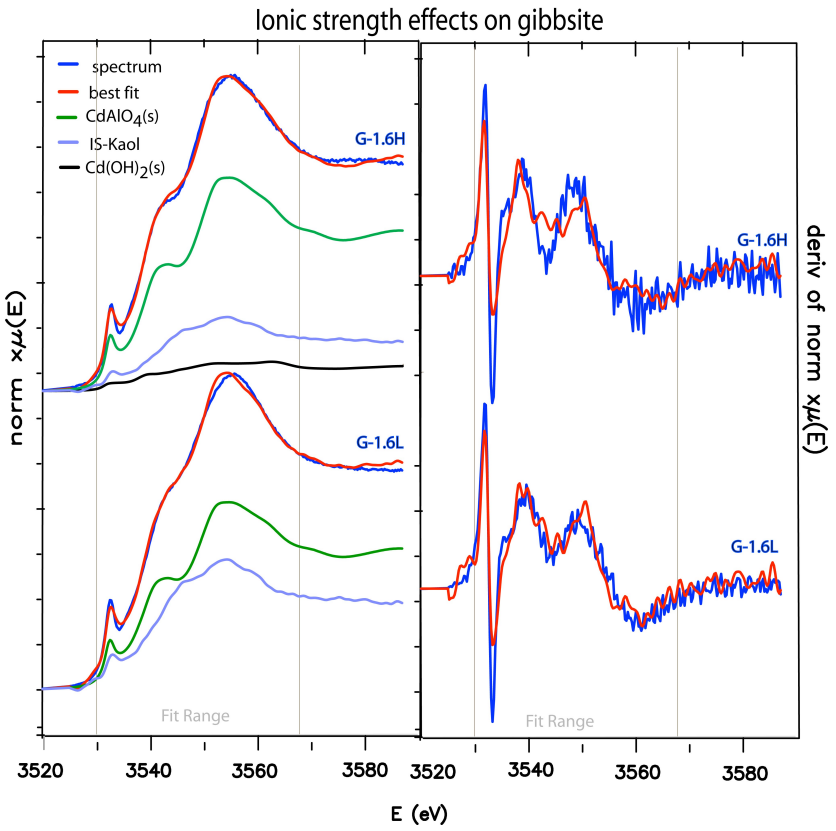
Ionic strength effects on gibbsite
spectrum
best fit
CdAlO4(s)
IS-Kaol
Cd(OH)2(s)
G-1.6H
G-1.6L
Fit Range
norm xμ(E)
deriv of norm xμ(E)
3520
3540
3560
3580
E (eV)

Figure 2.5

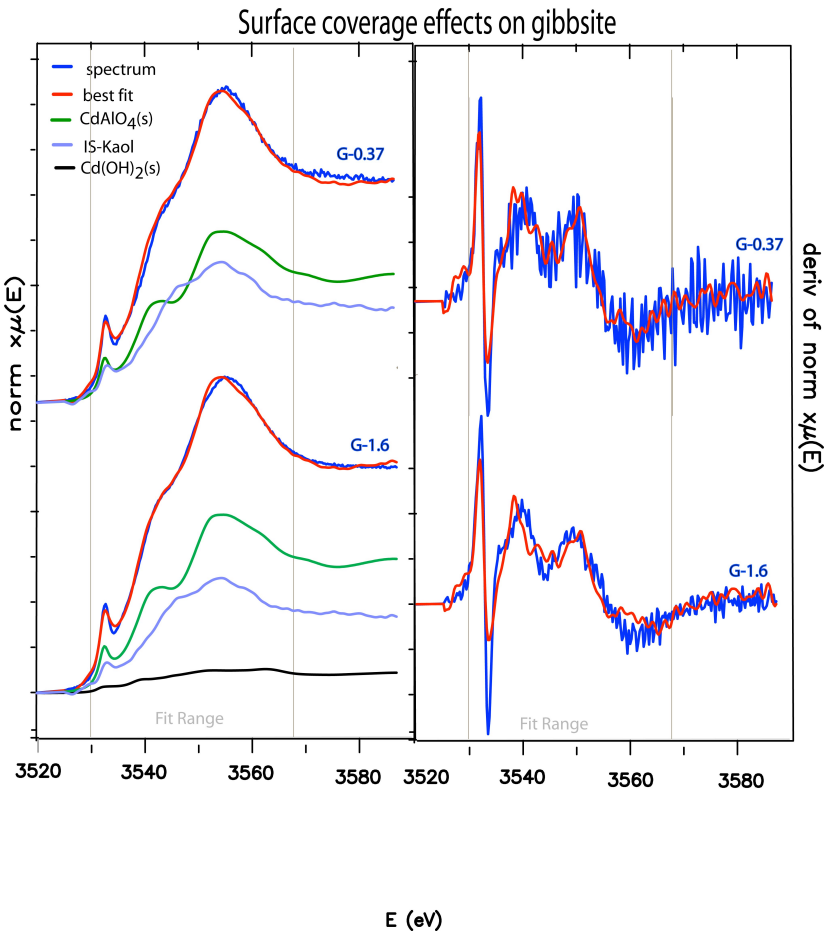
Surface coverage effects on gibbsite
spectrum
best fit
CdAlO4(s)
IS-Kaol
Cd(OH)2(s)
G-0.37
G-1.6
Fit Range
norm xμ(E)
deriv of norm xμ(E)
3520
3540
3560
3580
E (eV)

Figure 2.6

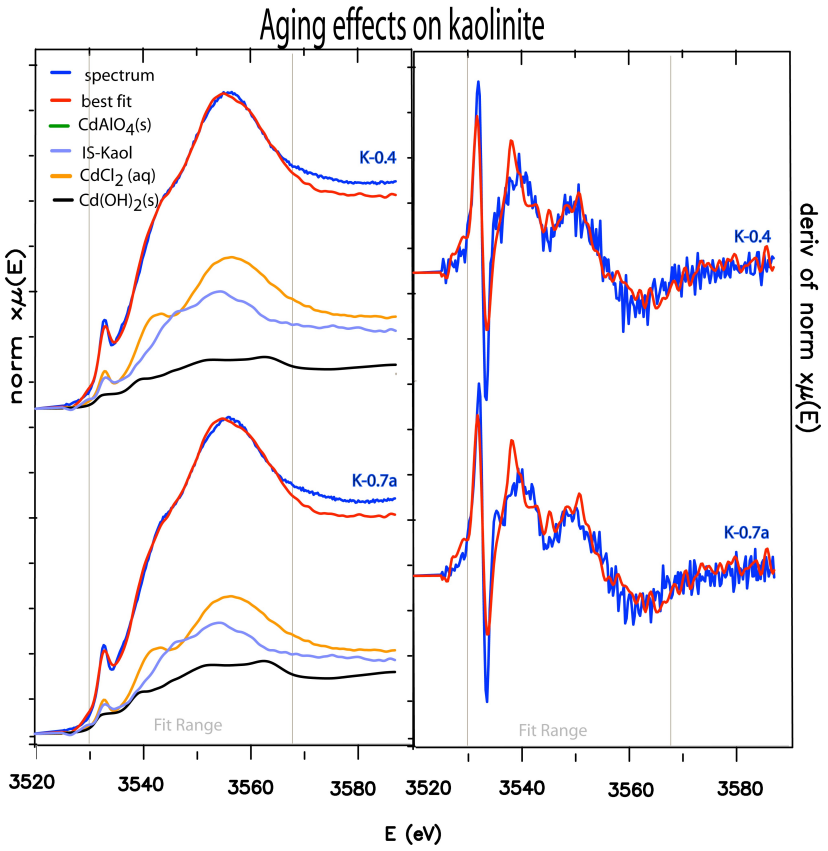
Aging effects on kaolinite
spectrum
best fit
CdAlO4(s)
IS-Kaol
CdCl2 (aq)
Cd(OH)2(s)
K-0.4
K-0.7a
Fit Range
norm xμ(E)
deriv of norm xμ(E)
3520
3540
3560
3580
E (eV)

Figure 2.7

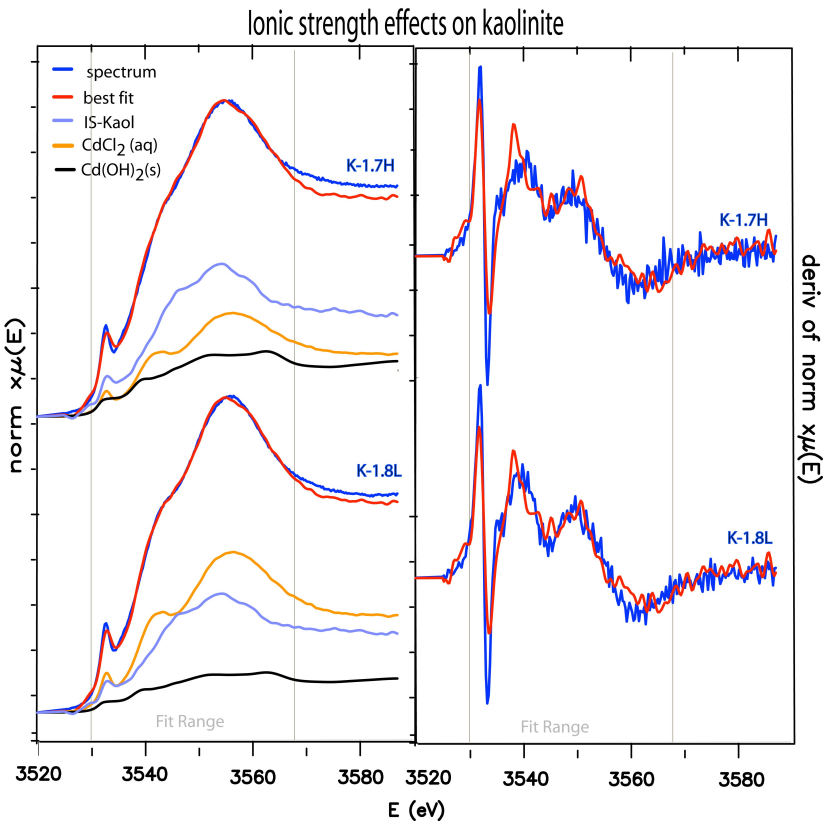
Ionic strength effects on kaolinite
spectrum
best fit
IS-Kaol
CdCl2 (aq)
Cd(OH)2(s)
K-1.7H
K-1.8L
Fit Range
norm xμ(E)
deriv of norm xμ(E)
3520
3540
3560
3580
E (eV)

Figure 2.8

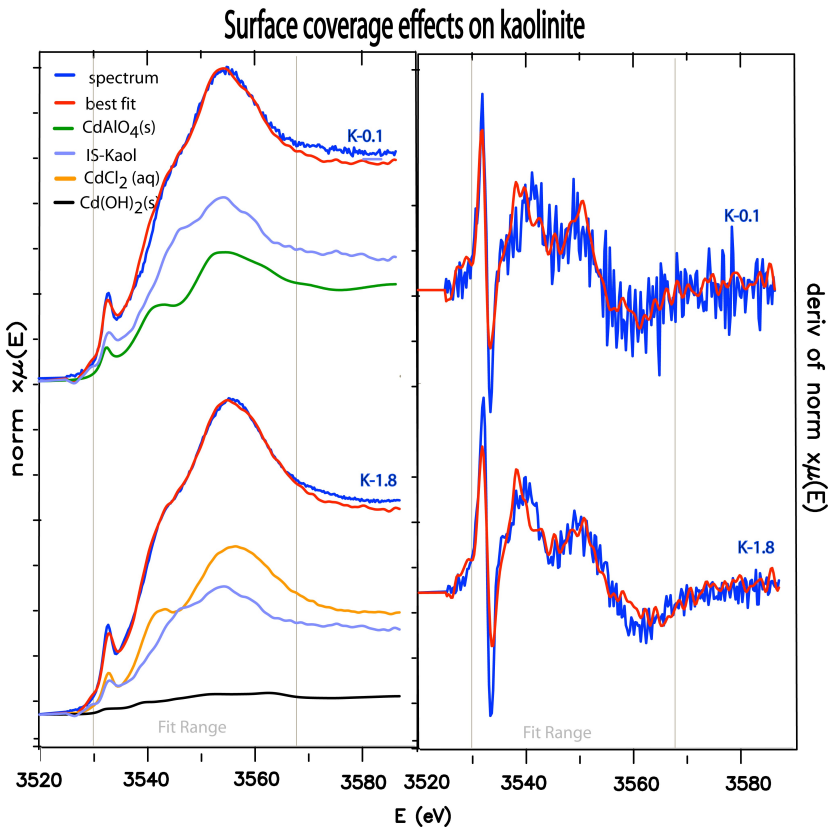
Surface coverage effects on kaolinite
spectrum
best fit
CdAlO4(s)
IS-Kaol
CdCl2 (aq)
Cd(OH)2(s)
K-0.1
K-1.8
Fit Range
norm xμ(E)
deriv of norm xμ(E)
3520
3540
3560
3580
E (eV)

Figure 2.9

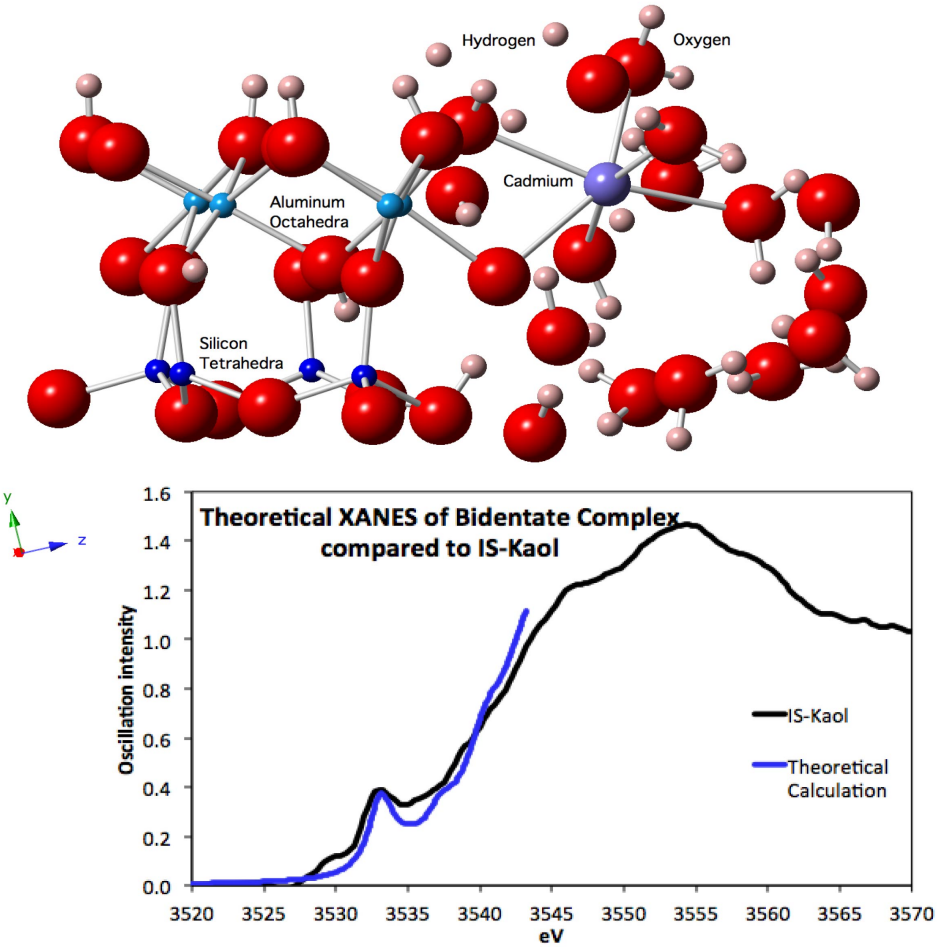
Hydrogen
Oxygen
Cadmium
Aluminum
Octahedra
Silicon
Tetrahedra
y
z
Theoretical XANES of Bidentate Complex
compared to IS-Kaol
Oscillation intensity
1.6
1.4
1.2
1.0
0.8
0.6
0.4
0.2
0.0
3520
3525
3530
3535
3540
3545
3550
3555
3560
3565
3570
eV
IS-Kaol
Theoretical
Calculation

Figure 2.10

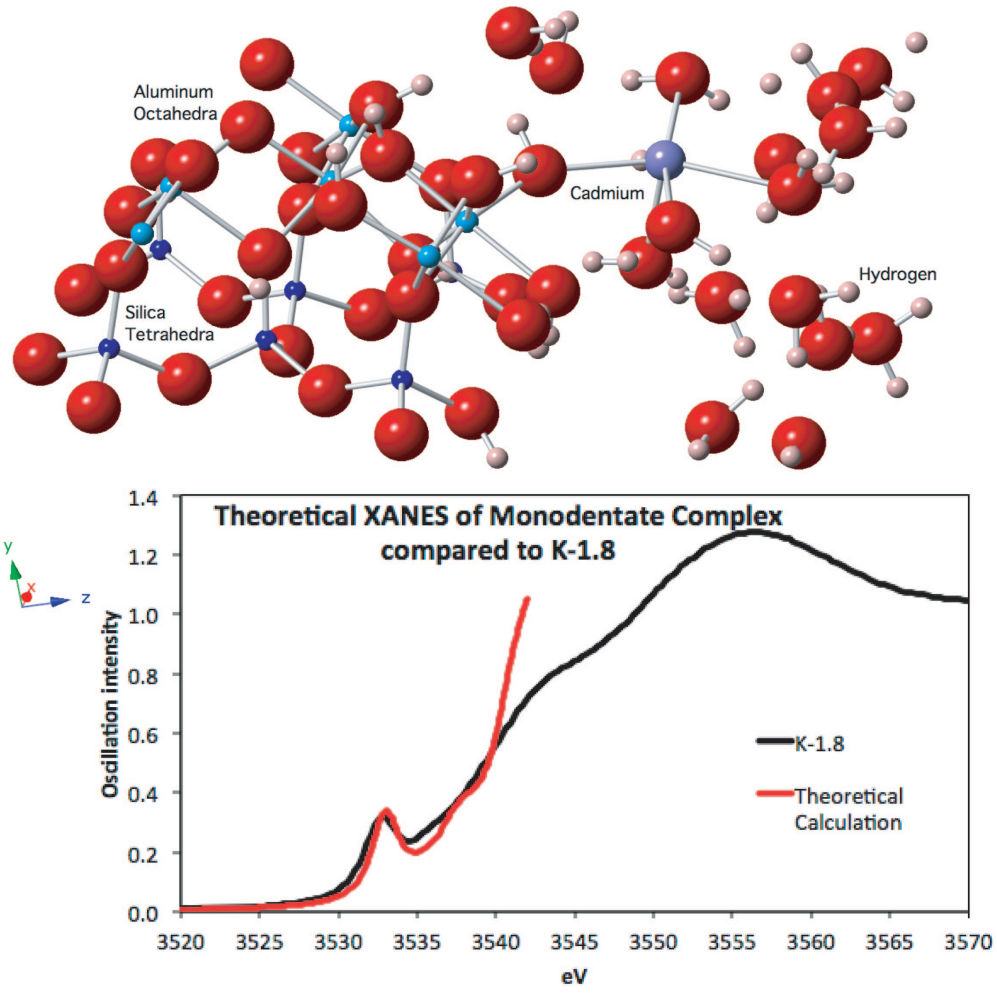
Aluminum
Octahedra
Cadmium
Hydrogen
Silica
Tetrahedra
Theoretical XANES of Monodentate Complex
compared to K-1.8
Oscillation intensity
eV
K-1.8
Theoretical
Calculation
1.4
1.2
1.0
0.8
0.6
0.4
0.2
0.0
3520
3525
3530
3535
3540
3545
3550
3555
3560
3565
3570
y
x
z

Figure 2.11

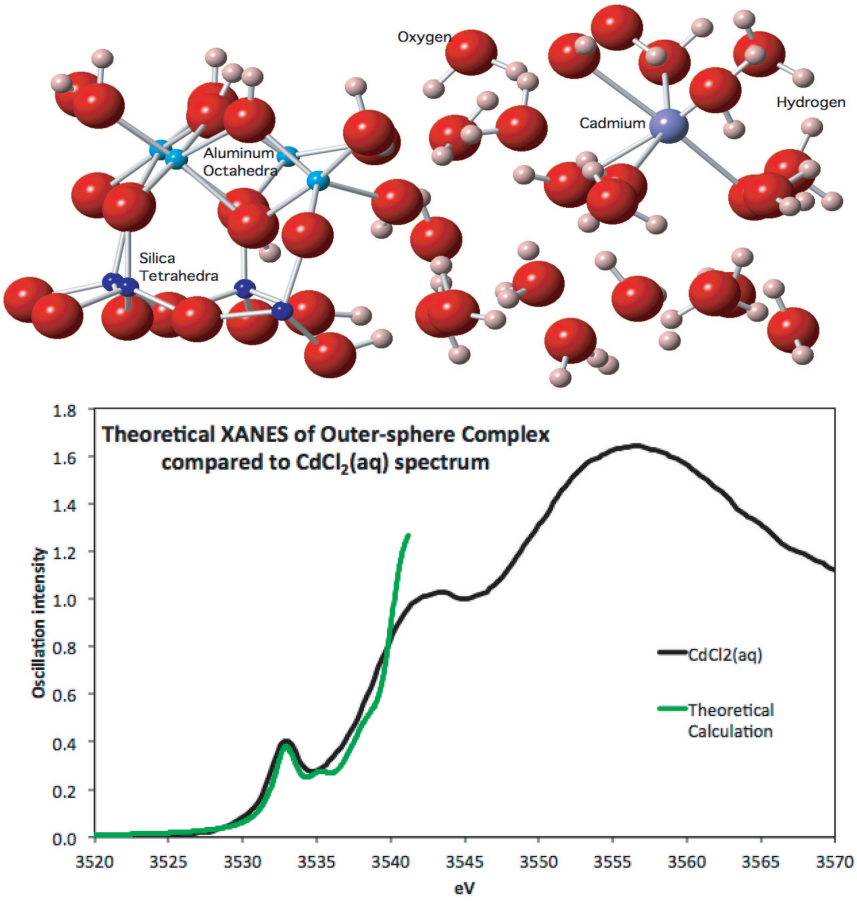
Oxygen
Hydrogen
Cadmium
Aluminum
Octahedra
Silica
Tetrahedra
Theoretical XANES of Outer-sphere Complex
compared to CdCl2(aq) spectrum
Oscillation intensity
eV
CdCl2(aq)
Theoretical
Calculation
0.0
0.2
0.4
0.6
0.8
1.0
1.2
1.4
1.6
1.8
3520
3525
3530
3535
3540
3545
3550
3555
3560
3565
3570

Figure 2.12

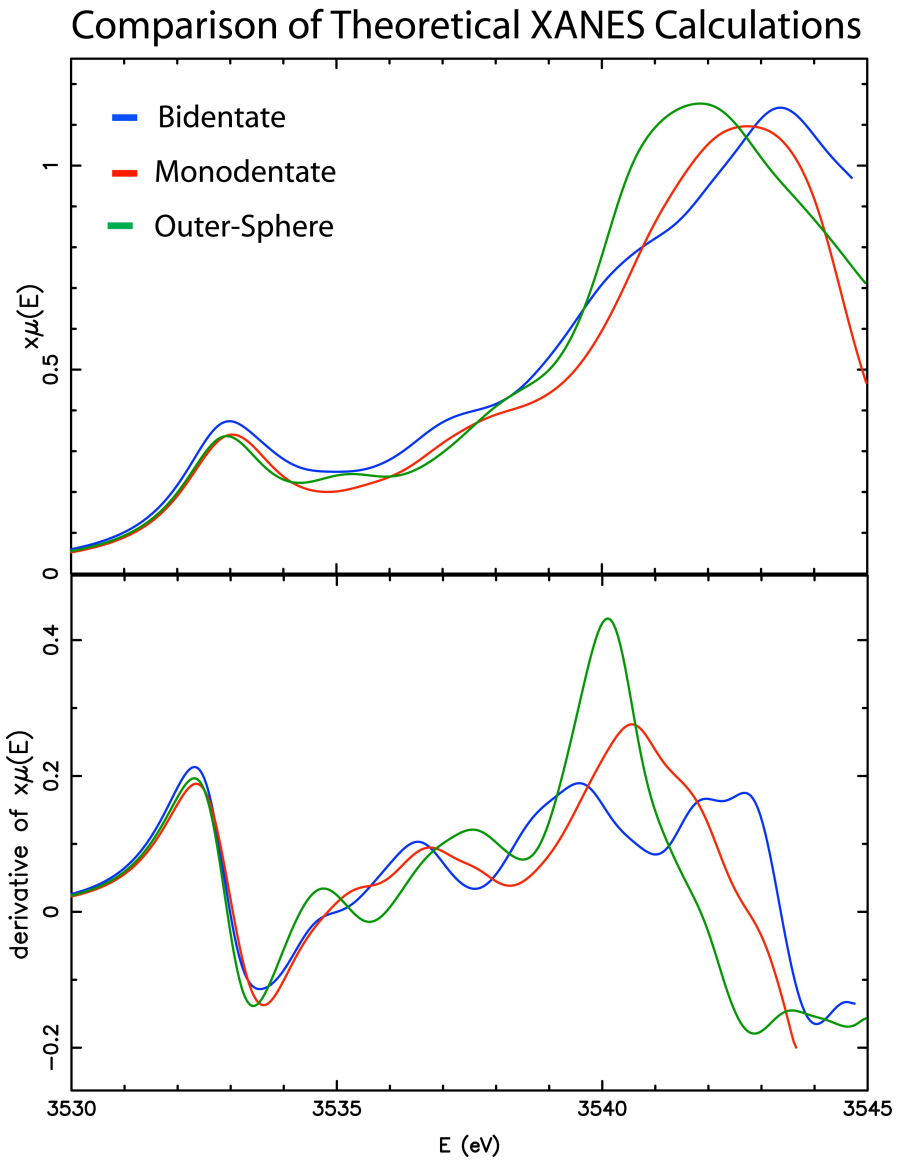
Comparison of Theoretical XANES Calculations
Bidentate
Monodentate
Outer-Sphere
xμ(E)
derivative of xμ(E)
E (eV)
0
0.5
1
−0.2
0
0.2
0.4
3530
3535
3540
3545

Figure 2.13

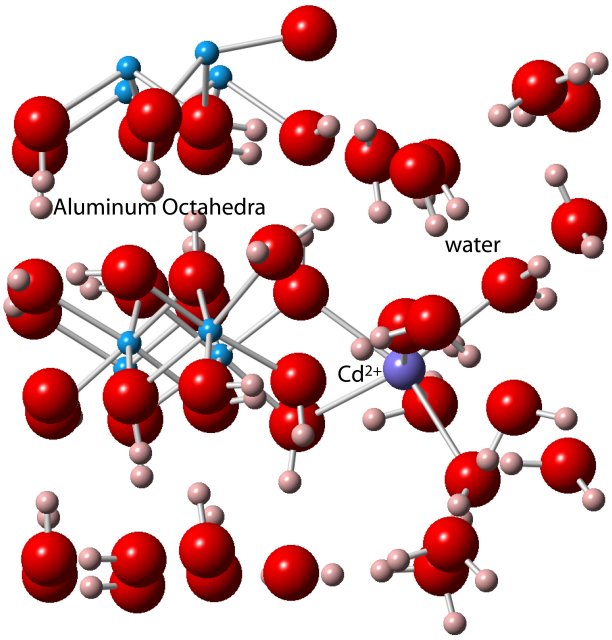

Figure 2.14

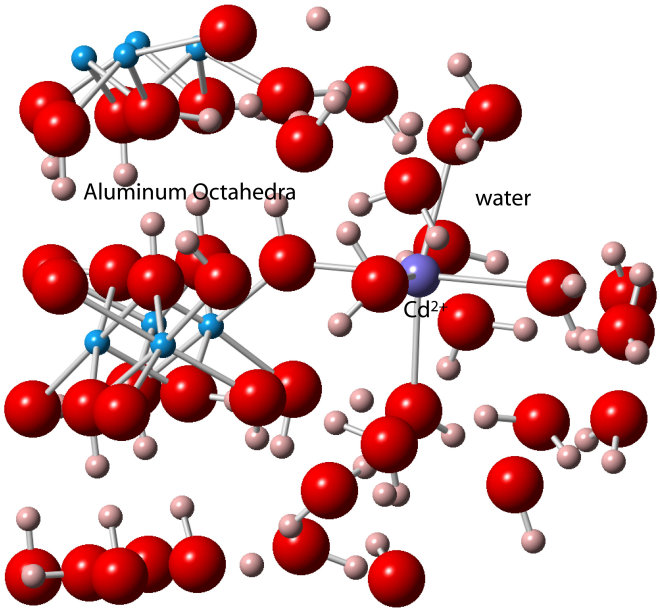

Figure 2.15

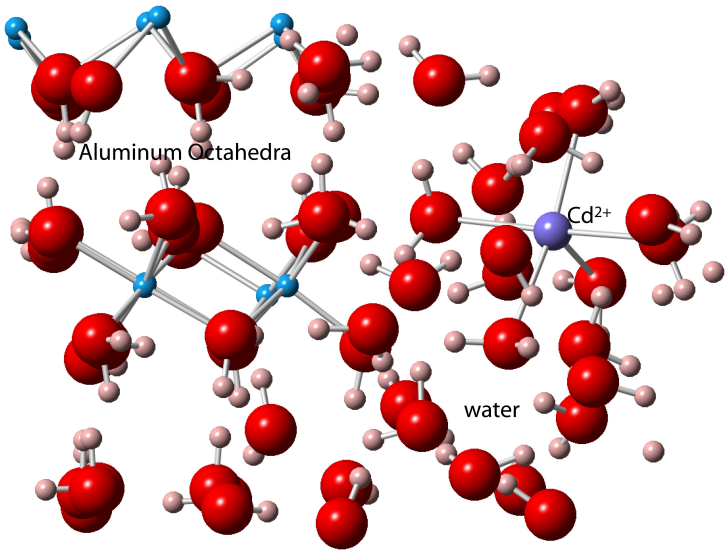

Figure 2.16

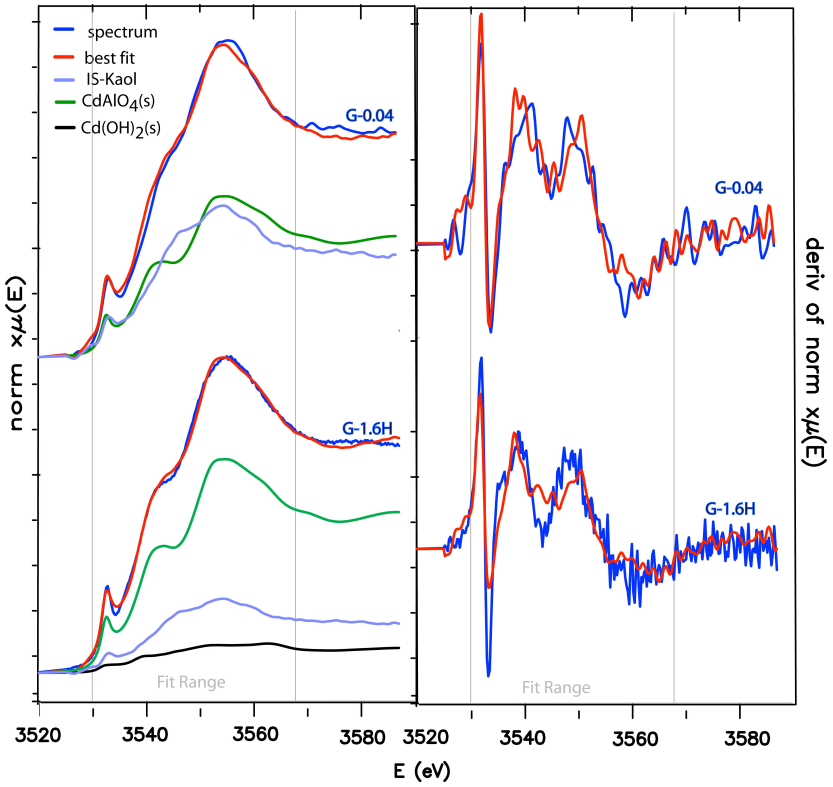
spectrum
best fit
IS-Kaol
CdAlO4(s)
Cd(OH)2(s)
G-0.04
G-1.6H
Fit Range
norm xμ(E)
deriv of norm xμ(E)
3520
3540
3560
3580
E (eV)

Figure 2.17

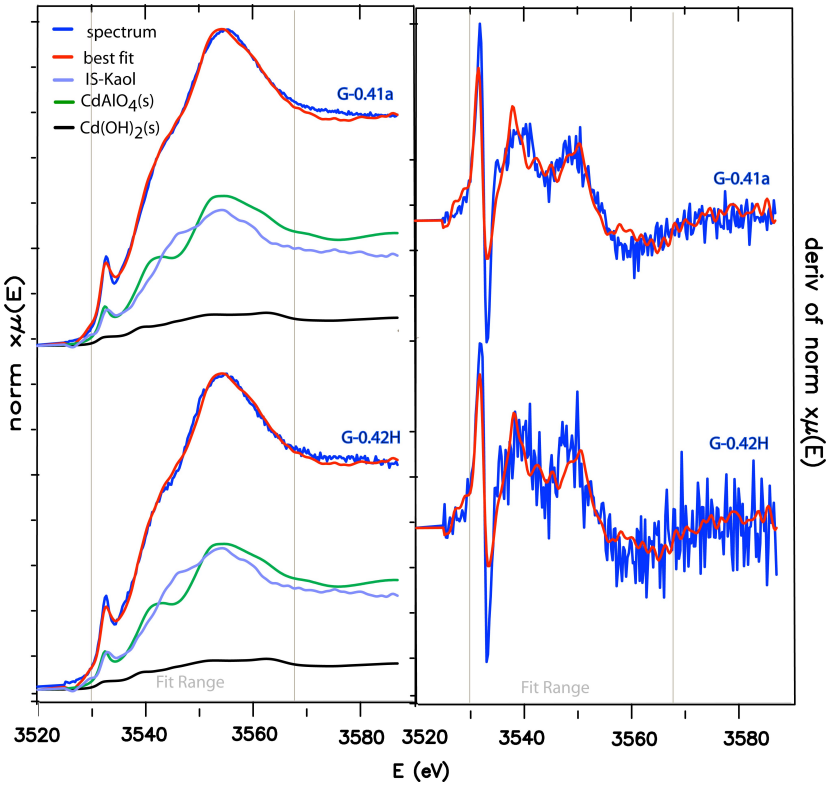
spectrum
best fit
IS-Kaol
CdAlO4(s)
Cd(OH)2(s)
G-0.41a
G-0.42H
Fit Range
norm xμ(E)
deriv of norm xμ(E)
3520
3540
3560
3580
E (eV)

Figure 2.18

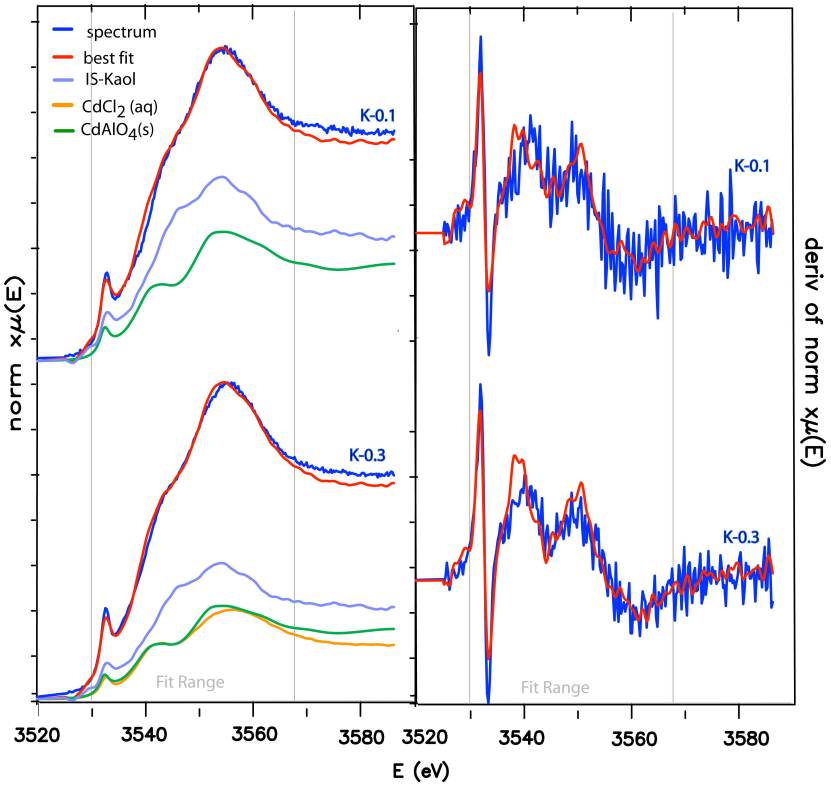
spectrum
best fit
IS-Kaol
CdCl2 (aq)
CdAlO4(s)
K-0.1
K-0.3
Fit Range
norm xμ(E)
deriv of norm xμ(E)
3520
3540
3560
3580
E (eV)

Figure 2.19

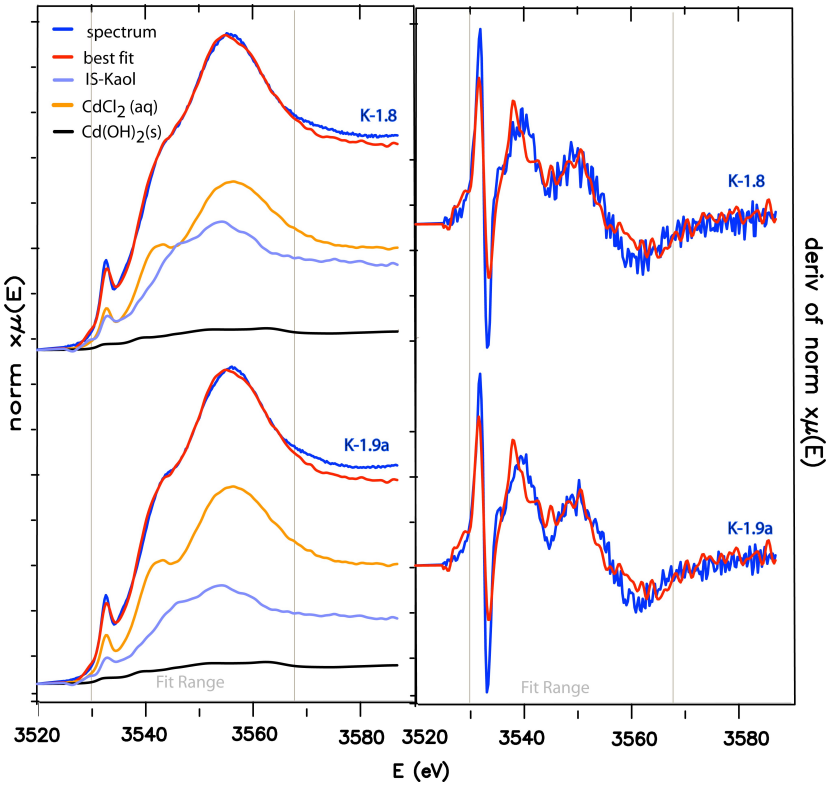

Figure 2.20

Figure 2.1.A-C

A. X-ray diffractogram of synthesized cadmium hydroxide and the cadmium hydroxide reference [a] (Poulsen et al.) **B.** X-ray diffractogram of synthesized cadmium hydroxychloride with Cd(OH)Cl reference [b](Visser, 1979). **C**. X-ray diffractogram of synthesized cadmium aluminate with several references. No cadmium aluminate reference could be found but the pattern can be explained by Hydrocalumite ($Ca_2Al(OH)_6Cl\cdot 2H_2O$) [c] (Fischer et al., 1980). Although there is no Ca in the Cd reference compound, we can infer that the crystal structure is similar to the layered hydroxide hydrocalumite.

Figure 2.2.

A summary of the references used initially in the linear combination fits of Cd^{2+} sorbed on kaolinite and gibbsite.

Figure 2.3.

IS-Kaol (Inner-Sphere Kaolinite) is the Cd^{2+} coverage spectrum that was collected on kaolinite. IS-Kaol spectrum (1Cd atom/125 nm^2) has unique features that could not be fit with linear combination.

Figure 2.4.

A comparison of aged and un-aged samples. G-1.6, equilibrated for 24 h in 30 mM ionic strength solution and G-1.9a, equilibrated for 36 d in 30 mM ionic strength solution. On the left are the normalized spectra, and the derivative of normalized spectra and linear combination fit are on the right. The IS-Kaol component represents an inner-sphere Cd^{2+} complex.

Figure 2.5.

A comparison of low and high ionic strength samples. G-1.6H, equilibrated for 24 h in 140 mM ionic strength solution and G-1.6L, equilibrated for 24 h in 14 mM ionic strength solution. On the left are the normalized spectra, and the derivative of normalized spectra and linear combination fit are on the right. The IS-Kaol component represents an inner-sphere Cd^{2+} complex.

Figure 2.6.

A comparison of low and high surface coverage samples. G-0.37, equilibrated for 24 h in 30 mM ionic strength solution, and G-1.6, also equilibrated for 24 h in 30 mM ionic strength solution. On the left are the normalized spectra, and the derivative of normalized spectra and linear combination fit are on the right. The IS-Kaol component represents an inner-sphere Cd^{2+} complex.

Figure 2.7.

A comparison of fresh and aged samples. K-0.4, equilibrated for 24 h in 30 mM ionic strength solution, and K-0.7a, equilibrated for 36 d in 30 mM ionic strength solution. On the left are the normalized spectra, and the derivative of normalized spectra and linear combination fit are on the right. The IS-Kaol component represents an inner-sphere Cd^{2+} complex.

Figure 2.8.

A comparison of high and low ionic strength samples. K-1.7H, equilibrated for 24 h in 140 mM ionic strength solution, and K-1.8L, equilibrated for 24 h in 24 mM ionic strength solution. On the left are the normalized spectra, and the derivative of normalized spectra and linear combination fit are on the right. The IS-Kaol component represents an inner-sphere Cd^{2+} complex.

Figure 2.9.

A comparison of low and high surface coverage samples. K-0.1, equilibrated for 24 h in 30 mM ionic strength solution, and K-1.8, also equilibrated for 24 h in 30 mM ionic

strength solution. On the left are the normalized spectra, and the derivative of normalized spectra and linear combination fit are on the right. The IS-Kaol component represents an inner-sphere Cd^{2+} complex.

Figure 2.10.

Above, a minimized DFT calculation featuring a bidentate Cd^{2+} complex occupying two aluminol sites on the (100) face of kaolinite. Below, the theoretical XANES calculated from the above structure and compared to "low" surface coverage kaolinite spectrum IS-Kaol, which has a surface coverage of 1 Cd/125 nm^2.

Figure 2.11.

Above, a minimized DFT calculation featuring a monodentate Cd^{2+} complex occupying one aluminol site on the (100) face of kaolinite. Below, the theoretical XANES calculated from the above structure and compared to "high" surface coverage kaolinite spectrum K-1.8, which has a surface coverage of 1 Cd/0.56 nm^2.

Figure 2.12

Above, a minimized DFT calculation featuring an outer-sphere Cd^{2+} complex on the (100) face of kaolinite. Below, the theoretical XANES calculated from the above structure and compared to $CdCl_2$(aq) reference used in linear combination fits as a proxy for outer-sphere complexes.

Figure 2.13

Comparison of theoretical XANES calculations from DFT simulations shown in Figures 2.10, 2.11, and 2.12.

Figure 2.14

DFT simulation of a bidentate Cd^{2+} complex on the (100) surface of Gibbsite.

Figure 2.15

DFT simulation of a monodentate Cd^{2+} complex on the (100) surface of Gibbsite.

Figure 2.16

DFT simulation of an outer-sphere Cd^{2+} complex on the (100) surface of Gibbsite.

Figure 2.17

Linear combination fits of gibbsite sorption samples G-0.04 and G-1.6H.

Figure 2.18

Linear combination fits of gibbsite sorption samples G-0.41a and G-0.42H.

Figure 2.19

Linear combination fits of kaolinite sorption samples K-0.1 and K-0.3.

Figure 2.20

Linear combination fits of kaolinite sorption samples K-1.8 and K-1.9a.

8. REFERENCES

Bradl, H.B., 2004. Adsorption of heavy metal ions on soils and soils constituents. Journal of Colloid and Interface Science 277, 1-18.

Brown, G.E., Henrich, V.E., Casey, W.H., Clark, D.L., Eggleston, C., Felmy, A., Goodman, D.W., Grätzel, M., Maciel, G., McCarthy, M.I., 1999. Metal oxide surfaces and their interactions with aqueous solutions and microbial organisms. Chemical Reviews 99, 77-174.

Chen, F., Hong, Y., Sun, J., Bu, J., 2006. Preparation and characterization of calcium aluminate by chemical synthesis. Journal of University of Science and Technology Beijing, Mineral, Metallurgy, Material 13, 82-86.

Choi, S., O'Day, P.A., Rivera, N.A., Mueller, K.T., Vairavamurthy, M.A., Seraphin, S., Chorover, J., 2006. Strontium speciation during reaction of kaolinite with simulated tank-waste leachate: Bulk and microfocused EXAFS analysis. Environmental Science & Technology 40, 2608-2614.

Crosson, G., Choi, S., Chorover, J., Amistadi, M.K., O'Day, P.A., Mueller, K.T., 2006. Solid-state NMR identification and quantification of newly formed aluminosilicate phases in weathered kaolinite systems. Journal of Physical Chemistry B 110, 723-732.

Fischer, R., Kuzel, H.J., Schellhorn, H., 1980. Hydrocalumit: Mischkristalle von Friedelschem salz 3CaOAl2O3*10H2O und tetracalciumaluminat-hydrat 3CaOAl2O3Ca(OH)2*10H2O. Neues Jahrb Mineral Monatsch H 7, 322-334.

Grafe, M., Singh, B., Balasubramanian, M., 2007. Surface speciation of Cd(II) and Pb(II) on kaolinite by XAFS spectroscopy. Journal of Colloid and Interface Science 315, 21-32.

Grim, R., 1962. Applied Clay Mineralogy. McGraw-Hill, New York.

Gu, X., Evans, L.J., 2008. Surface Complexation modelling of Cd(II), Cu(II), Ni(II), Pb(II) and Zn(II) adsorption onto kaolinite. Geochimica Et Cosmochimica Acta 72, 267-276.

Hiemstra, T., deWit, J.C.M., Van Riemsdijk, W.H., 1989a. Multisite proton adsorption modeling at the solid/solution interface on (hydr) oxides—A new approach: II.

Application to various important (hydr) oxides. Journal of Colloid and Interface Science 133, 105-117.

Hiemstra, T., Van Riemsdijk, W., 1991. Physical chemical interpretation of primary charging behaviour of metal (hydr) oxides. Colloids and surfaces 59, 7-25.

Hiemstra, T., Yong, H., Van Riemsdijk, W., 1999. Interfacial charging phenomena of aluminum (hydr) oxides. Langmuir 15, 5942-5955.

Isaure, M.-P., Fayard, B., Sarret, G., Pairis, S., Bourguignon, J., 2006. Localization and chemical forms of cadmium in plant samples by combining analytical electron microscopy and X-ray spectromicroscopy. Spectrochimica Acta Part B: Atomic Spectroscopy 61, 1242-1252.

Jalilehvand, F., Leung, B.O., Mah, V., 2009. Cadmium (II) complex formation with cysteine and penicillamine. Inorganic chemistry 48, 5758-5771.

Kresse, G., Furthmüller, J., 1996. Efficient iterative schemes for ab initio total-energy calculations using a plane-wave basis set. Physical Review B 54, 11169–11186.

Kresse, G., Furthmüller, J., Hafner, J., 1994. Theory of the crystal structures of selenium and tellurium: The effect of generalized-gradient corrections to the local-density approximation. Physical Review B 50, 13181-13185.

Kresse, G., Hafner, J., 1993. Ab initio molecular dynamics for open-shell transition metals. Physical Review B 48, 13115-13118.

Kresse, G., Hafner, J., 1994. Ab initio molecular-dynamics simulation of the liquid-metal-amorphous-semiconductor transition in germanium. Physical Review B 49, 14251-14269.

Kubicki, J., Apitz, S., 1998. Molecular cluster models of aluminum oxide and aluminum hydroxide surfaces. American Mineralogist 83, 1054-1066.

Lopata, K., Van Kuiken, B.E., Khalil, M., Govind, N., 2012. Linear-response and real-time time-dependent density functional theory studies of core-level near-edge X-ray absorption. Journal of Chemical Theory and Computation 8, 3284-3292.

Luo, L., Ma, C., Ma, Y., Zhang, S., Lv, J., Cui, M., 2011. New insights into the sorption mechanism of cadmium on red mud. Environmental Pollution 159, 1108-1113.

Pickering, I.J., Prince, R.C., George, G.N., Rauser, W.E., Wickramasinghe, W.A., Watson, A.A., Dameron, C.T., Dance, I.G., Fairlie, D.P., Salt, D.E., 1999. X-ray absorption spectroscopy of cadmium phytochelatin and model system. Biochimica et biophysica acta 1429, 351-364.

Poulsen, K., Henslee, Company, D.C., Private Communication.

Ravel, B., Newville, M., 2005. ATHENA, ARTEMIS, HEPHAESTUS: data analysis for X-ray absorption spectroscopy using IFEFFIT. Journal of synchrotron radiation 12, 537-541.

Serrano, S., O'Day, P.A., Vlassopoulos, D., Garcia-Gonzalez, M.T., Garrido, F., 2009. A surface complexation and ion exchange model of Pb and Cd competitive sorption on natural soils. Geochimica Et Cosmochimica Acta 73, 543-558.

Siebers, N., Kruse, J., Eckhardt, K.-U., Hu, Y., Leinweber, P., 2012. Solid-phase cadmium speciation in soil using L3-edge XANES spectroscopy with partial least-squares regression. Journal of synchrotron radiation 19, 579-585.

Srivastava, P., Singh, B., Angove, M., 2005. Competitive adsorption behavior of heavy metals on kaolinite. Journal of Colloid and Interface Science 290, 28-38.

Stern, O., 1924. Theory of the electrical double layer.(In German.). Electrochemistry 30, 508-516.

Valiev, M., Bylaska, E.J., Govind, N., Kowalski, K., Straatsma, T.P., Van Dam, H.J., Wang, D., Nieplocha, J., Apra, E., Windus, T.L., 2010. NWChem: a comprehensive and scalable open-source solution for large scale molecular simulations. Computer Physics Communications 181, 1477-1489.

Van Kuiken, B.E., Valiev, M., Daifuku, S.L., Bannan, C., Strader, M.L., Cho, H., Huse, N., Schoenlein, R.W., Govind, N., Khalil, M., 2013. Simulating Ru L3-Edge X-ray Absorption Spectroscopy with Time-Dependent Density Functional Theory: Model Complexes and Electron Localization in Mixed-Valence Metal Dimers. The Journal of Physical Chemistry A 117, 4444-4454.

Vasconcelos, I.F., Haack, E.A., Maurice, P.A., Bunker, B.A., 2008. EXAFS analysis of cadmium (II) adsorption to kaolinite. Chemical Geology 249, 237-249.

Visser, J., 1979. Technisch physische dienst. Delft, The Netherlands.

Weerasooriya, R., Dharmasena, B., Aluthpatabendi, D., 2000. Copper-gibbsite interactions: an application of 1-pK surface complexation model. . Colloids and Surfaces A: Physicochemical and Engineering Aspects 170.

Weerasooriya, R., Wijesekara, H., Bandara, A., 2002. Surface complexation modeling of cadmium adsorption on gibbsite. Colloids and Surfaces a-Physicochemical and Engineering Aspects 207, 13-24.

Chapter 3: Aqueous Cd^{2+} Sorption on Kaolinite and Gibbsite

ABSTRACT

Distinguishing reactive surface area, a measure of the functional groups that participate in molecular-scale surface reactions, from geometric surface area is important in the accurate description of environmental processes involving mineral surfaces. In this study, surface complexation modeling of aqueous cadmium (Cd^{2+}) sorption onto kaolinite and gibbsite was constrained by results from Cd L_{III} X-ray Absorption Near Edge Structure (XANES) and periodic density functional theory (DFT) calculations to better quantify surface binding sites at the molecular scale. Batch sorption experiments with kaolinite or gibbsite were performed at different metal ($CdCl_2$) and background electrolyte ($CaCl_2$) concentrations. Samples were equilibrated for 24 h at constant pH, centrifuged, and supernatant solutions removed. Filtered solutions were analyzed by ICP-OES and the adsorbed fraction of metal was calculated by difference. Periodic DFT results were used to estimate the relative energies of each surface complex cluster and interatomic distances (see Chapter 2). The Charge Distribution MUlti-SIte Complexation (CD-MUSIC) model was used in PhreePlot with a constrained set of reactions and used to derive conditional equilibrium constants for surface complexation reactions. Cadmium sorption on gibbsite was fit with a mononuclear bidentate reaction at low surface coverage (1 Cd/300 nm^2), and with bidentate and dimer reactions at high coverage (1 Cd/3 nm^2). Cadmium sorption on kaolinite was fit with a bidentate reaction at low surface coverage (1 Cd/150 nm^2), and with bidentate, monodentate, and outer-sphere reactions at high surface coverage (1 Cd/1.5 nm^2). The results indicate that bidentate

complexes form first on both kaolinite and gibbsite. With increased surface coverage, dimer complexes form on gibbsite, and outer-sphere complexes form on kaolinite, reinforcing interpretations from XANES linear combination fits which informed our surface complexation model.

1. INTRODUCTION

Mineral-water interface reactions such as dissolution, precipitation, nutrient-fixation, and sorption, are some of the most important reactions on Earth. Mineral surfaces are involved in all these reactions, but only a portion of the physical surface area is actually participating in the reactions. This is the reactive surface area. Adsorption is accumulation of matter at the solid-solution interface (Stumm and Morgan, 1996), a process highly dependent upon pH and concentration of "matter," in this case aqueous Cd^{2+}. Kaolinite is a well-defined clay mineral consisting of a tetrahedrally coordinated silica layer and an octahedrally coordinated alumina layer. Kaolinite has no cation exchange capacity, and any cation exchange capacity in natural kaolinite comes from a smectite impurity (Sposito, 1984). Gibbsite is a metal hydroxide mineral, and resembles the octahedrally coordinated alumina layer in kaolinite. Gibbsite, like kaolinite, lacks cation exchange capacity, making it an excellent choice for researching reactive surface area (Yang et al., 2007). Hydroxylated sites on kaolinite and gibbsite control sorption reactions, which can be investigated using sorption experiments.

Cadmium is a toxic, commonly divalent, transition metal that is used in batteries and plastics. Cd^{2+} is also a common contaminant in fertilizers, and a byproduct of zinc mining and other mining endeavors (A.T.S.D.R., 2008). Chronic exposure to Cd^{2+} can

cause kidney disease, developmental issues, and reproductive harm (U.S.E.P.A., 1992). Cd^{2+} is a particularly "hard," or ionic, cation, and as an end member of cation-behavior is an appropriate choice for probing mineral surfaces.

Although many studies have used surface complexation modeling in order to constrain the stoichiometry and reactivity of surface complexes on kaolinite and gibbsite (Gu and Evans, 2008; Serrano et al., 2009; Srivastava et al., 2005; Weerasooriya et al., 2000), predictions of surface complex stoichiometry is often based on results from surface complex modeling. In order to understand changes in surface complexation across orders of magnitude change in surface coverage and solution condition, it is helpful constrain surface complexation modeling with other types of data. Studies by Machesky et al. (2008) and Zhang et al. (2004) combine surface complexation modeling with periodic Density Functional Theory (DFT) calculations. Cd L_{III} XANES spectroscopy is sensitive to the local bonding environment of the adsorbing Cd^{2+} (see Chapter 2), and DFT calculations can provide the energetics and stoichiometry of probable surface complexes. Additionally, clusters of likely surface complexes can be extracted from DFT calculations and used in theoretical XANES calculations. Theoretical XANES are then compared to the experimentally collected XANES of similar surface coverage for comparison of features. Using multiple methods to analyze surface complexation enables cross-referencing of data and has the potential to constrain surface complex stoichiometry and surface reactivity across large changes in surface coverage and solution conditions.

1.1 Summary of the Charge Distribution MUlti-SIte Complexation Model

The CD-MUSIC model (Hiemstra et al., 1989a; Hiemstra et al., 1989; Hiemstra and Van Riemsdijk, 1996; Van Riemsdijk and Hiemstra, 2006) is a combination of two approaches to interpreting surface chemistry: the multi-site model and charge distribution. The multi-site complexation model, or MUSIC model, is the application of Pauling's bond valence rules to the charged mineral surface (Pauling, 1949), where the valence (*v*) is equal to the charge (*z*) of the metal in the hydroxide mineral divided by the coordination number (*CN*)

Equation 1 $$v = \frac{z}{\mathrm{CN}}$$

The MUSIC model is a one-pK model, meaning that only one protonation step is considered, ($\equiv AlOH^{0.5-} + H^{+} \rightarrow \equiv AlOH_2^{0.5+}$) and the pK is equal to the point of zero charge (PZC) of the mineral in question (Van Riemsdijk and Hiemstra, 2006). In the classic two-pK, or two-step protonation model, only one type of surface site can be considered, which will only be reactive over a finite pH range. The surface, z_1, and z_2 layers (layers 1 and 2 in Figure 3.1) make up the "Three Plane Model" (TP), derived from the basic Stern model (Stern, 1924). Solution counter ions are not allowed to approach closer than the Stern layer, which can be considered z_2. The total capacitance of the stern layer (C_T) can be defined as:

Equation 2 $$\frac{1}{C_T} = \frac{1}{C_1} + \frac{1}{C_2}$$

Where C_1 is the capacitance of the inner layer and C_2 is the capacitance of the outer layer. C_T is equal to 0.9 F/m^2 when C_1=1.1 F/m^2 and C_2=5 F/m^2 (Hiemstra and Van Riemsdijk, 1991)

The CD-MUSIC and TP models attempt to make the modeling of sorption behavior realistic and feasible. The CD and TP models consider that large, specifically adsorbing ions must take up some space on the surface and cannot be reduced to point charges. Solution counter-ions can be reduced to point charges because there is infinite space in solution. The MUSIC model uses Pauling's bond valence rules to attribute charge to the surface, and the one-pK model that allows for multiple binding sites, maintaining that a particular surface group will only be reactive over a certain range in pH (Hiemstra et al., 1989a; Hiemstra et al., 1989). The CD-MUSIC model will be used to regress complexation constants for Cd^{2+} adsorption on kaolinite and gibbsite.

2. METHODOLOGY

2.1 Materials

2.1.1 Reagents

De-ionized water (18.2 MΩ-cm, Milli-Q+, Millipore) sparged with N_2 for 8-12 h to remove dissolved CO_2 was used for all solutions. All chemical salts used were reagent grade or better, and purified no further. Solutions were stored in polypropylene containers that had been washed in 2% HNO_3. Cadmium (Cd^{2+}) stock solutions were made from $CdCl_2$ (Sigma Aldrich 99.99% pure).

2.1.2 Kaolinite and Gibbsite Preparation and Characterization

Kaolinite (KGa-2) from Warren County, Georgia was obtained through the Clay Minerals Society. Kaolinite (50 ± 2 g) was mixed with 250 g of water and adjusted to pH 9.5±0.1 to promote dispersion. The slurry was stirred for 45 min and then transferred into 250 ml centrifuge bottles. Serial centrifugations of 5 min at 47 RCF were performed,

removing and preserving the <4 μm fraction in the supernatant solution in each repetition. This process was repeated until the supernatant was clear. The <4 μm kaolinite fraction was washed by adding 1.0 M NaCl solution adjusted to pH 3 with 1.0 M HCl, stirring for 20 min, and then centrifuging for 5 min at 24,000 g and decanting the supernatant. This was repeated until the slurry was approximately pH 3 (5-6 repetitions). The slurry remained at pH 3 for no longer than 2 h to minimize mineral dissolution. The kaolinite was then washed with a pH 7 0.01 M NaCl solution by the same process explained above until the slurry reached approximately pH 6. The slurry was mixed with ultra-pure water, centrifuged, and supernatant decanted to remove NaCl. The slurry was mixed with a 0.01 M $CaCl_2$ solution, centrifuged, and supernatant decanted. Washed clay was then equilibrated with 0.01 M or 0.001 M $CaCl_2$ solution and readjusted to pH 6 if necessary. The headspace in the container was blown off with N_2 before capping, and then the slurry was homogenized overnight on a horizontal rotator at 100 RPM. Mineral slurries were stored at 4°C.

Gibbsite (Micral 916) from Huber Engineered Materials, was size separated and cleaned in a similar fashion to the kaolinite. Instead of a pH 7, 0.01 M NaCl solution, pH 8 was used. The final gibbsite slurry was adjusted to pH 7 to minimize mineral dissolution.

After homogenization of the mineral slurry, a drying experiment was performed to determine the solid:liquid ratio in the slurry. The mineral slurry was stirred for 1 h at room temperature to ensure homogenization before taking five 1-ml aliquots. Aliquots were placed in pre-weighed polypropylene sample containers, and then weighed again.

Samples were dried in a 60°C oven for 24 h. Three controls were included in the drying to ensure no mass loss from the sample cups due to volatilization. After drying sample cups were re-weighed and mass loss was determined by difference. Dry mass:solution volume ratios in the slurries were targeted to be 1 g /10 ml.

Solids were measured for specific surface area and particle size distribution. Specific surface area was measured on dried solids (60°C oven for 24 h) using a BET (Brunauer, Emmett, Teller) surface area analyzer (Micromeritics TriStar 3000) with N_2 gas with <0.5% error for KGa-2 kaolinite and Micral 916 gibbsite.

Particle size distribution was measured using Dynamic Laser Scattering (DLS) with Brookhaven Instruments BI-9000AT. The mineral slurry was stirred for 1 h prior to taking a 1 ml aliquot, placing in an Eppendorf tube, and sonicating for several hours. Ten µl of slurry was then diluted in 6 ml of DI water in a glass scintillation vial. The vial was placed in the DLS instrument and measured at a wavelength of 633 nm with a 10 µs measurement delay.

X-ray diffraction (XRD) was performed in the Imaging and Microscopy Facility at the University of California, Merced. Powder mounts of dried solids were prepared on zero-background silica plates. Diffractograms were collected with a PanAnalytical X'Pert PRO diffractometer with an ultra-fast X'Celerator detector from 2°-70° 2θ with step size of 0.002° and count time of 10 s using CoKα radiation.

2.2 Batch Experiments

Batch metal sorption experiments of Cd^{2+} on kaolinite or gibbsite were carried out in pre-weighed, trace-metal free polypropylene copolymer centrifuge tubes (Nalgene). Before beginning, the mineral slurry (kaolinite or gibbsite depending on the experiment) was stirred for 1 h. While stirring continuously, a predetermined aliquot of mineral slurry was transferred to each centrifuge tube. Tubes were reweighed after every addition (±0.2 mg). An aliquot of 0.1 M, 0.01 M, or 0.001 M $CaCl_2$ solution was added to the mineral slurry and allowed to equilibrate for 2 h on an end-over-end rotator at 26 RPM. A pre-determined volume of 0.01 M $CdCl_2$ was then added, and pH was adjusted with 0.01 and 0.1 M NaOH and HCl to a target value for each tube using Cole Parmer Accumet combination reference electrode, model 55500-04. After pH adjustment and re-weighing, samples were replaced on the end-over-end rotator and equilibrated for ~10 h at 26 RPM. The pH was readjusted for each tube and the mass was measured for the last time. After a total of 24 h of reaction, the final pH was measured and samples were centrifuged at 27,000 RCF for 20 min (kaolinite) or 35,000 RCF for 40 min (gibbsite). The supernatant was removed and 3-5 ml was passed through a 0.22 μm Whatman polypropylene with glass microfiber filter. Filtered solutions were analyzed by ICP-OES (Perkins-Elmer Optima 5300dv). Limit of quantitation for Cd^{2+} was calculated to be 14 ppb. Above the limit of quantitation, analytical error is $\leq \pm 2\%$. Final sorption densities were calculated by difference from the original Cd^{2+} concentration and the dry weight of the solid. Reacted solids were stored in trace-metal free polypropylene centrifuge tubes. Parallel experiments were performed for kaolinite and gibbsite over pH values 3-8 under the conditions listed in the Appendix, Tables A1-A2. Aqueous Al and Ca were also

measured, with limits of quantitation at 40 ppb (mg/L) and 22 ppb (mg/L). Above the limit of quantitation, analytical error is ≤ ±2%.

2.3 Modeling and Regression of Complexation Constants

2.3.1 Model Formulation

DFT calculations on kaolinite have shown that Cd^{2+} complexes are most favorable on aluminol sites, and XANES linear combination fits also confirmed that inner-sphere complexes are interacting with Al. Therefore, only aluminol sites were considered in the surface complexation modeling of kaolinite. The stoichiometry of surface complexes was constrained by evidence from periodic density calculations executed by the Vienna Ab-initio Simulation Package (VASP) (Kresse and Furthmüller, 1996; Kresse and Hafner, 1993) and evidence from linear combination XANES calculations discussed in Chapter 2. From XANES calculations, it is apparent that inner-sphere complexes and dimer complexes are necessary for both kaolinite and gibbsite samples. XANES results also indicate that an outer-sphere complex should be included for kaolinite, as well as some consideration of surface reformation for gibbsite.

From DFT calculations, bidentate and monodentate reactions are favorable on the gibbsite (100) surface (0 and 6 kJ/mol respectively), as well as a dimer complex at slightly higher energy (37 kJ/mol). On the kaolinite (100) surface, monodentate and outer-sphere complexes are the most energetically favorable (0 and 9 kJ/mol respectively), while the dimer complex had a higher enthalpy at 68 kJ/mol.

Monodentate, bidentate, and dimer reactions were included for the gibbsite model. Monodentate, bidentate, dimer, and outer-sphere reactions were considered for the kaolinite model (Table 3.1).

Site densities are taken from crystallographic estimations in the literature for kaolinite (Brady et al., 1996) and gibbsite (Hiemstra et al. 1989a). Only the (100) face of kaolinite was considered in this simulation, since the (001) face is relatively non-reactive and characterized by non-pH dependent permanently charged sites created by isomorphic substitution (Gu and Evans, 2008).

2.3.2 PhreePlot

The Charge Distribution MUlti-SIte Complexation (CD-MUSIC) model was chosen to describe Cd^{2+} sorption because of its flexibility to include multiple sites and surfaces, and the ability to include information such as bond distances in the model. Partial charges z0 and z1 were fixed, using the bond valence model and 6-fold coordination with the adsorption of a Cd^{2+} cation (Pauling, 1949).

Experimental uptake curves were used to fit conditional equilibrium surface complexation constants using the program PhreePlot (Kinniburgh and Cooper, 2011). Two surface coverage loadings were modeled for each mineral, separated by two orders of magnitude. Firstly, the "low coverage" model was executed with uptake curves from experiments G-22 and K-25, with surface loadings of 1 Cd/300 nm^2 on gibbsite, and 1 Cd/150 nm^2 on kaolinite. Secondly, the "high coverage" model was performed with uptake curves from experiments G-23 and K-26, with surface loadings of 1 Cd/3 nm^2 on gibbsite, and 1 Cd/1.5 nm^2 on kaolinite. Surface area, site density, capacitances, and

aqueous complexes are summarized in Table 3.2. See Tables 3.3 and 3.4 in Appendix I for experimental conditions of G-22, G-23, K-25, and K-26. With the hypothesis that the bidentate complex will be the primary surface complex at low surface coverage, a bidentate reaction was the sole fitted parameter in the low coverage model. At high surface coverage, different surface complexes may be necessary to accommodate additional Cd^{2+}. The fitted bidentate equilibrium constant from the low coverage model was used as a fixed parameter in the high coverage model and plausible monodentate, dimer, and outer-sphere complexes, as constrained by XANES linear combination fits and DFT calculations, are fit simultaneously. Fit parameters were also modeled with PHREEQC (Parkhurst and Appelo, 1999). The wateq4f database was used in PHREEQC updated with constants from Powell et al. (2011).

3. RESULTS

3.1 Mineral Characterization

Two different kaolinite batches were cleaned and characterized by N_2 BET. Surface area for kaolinite (KGa-2) was between 16 and 18 m^2/g, and between 23 and 26 m^2/g for gibbsite. XRD results verified the identity of the kaolinite and gibbsite phases and also show that there is no excess NaCl in the mineral slurry (Figure 3.2 A and B). Particle size distributions from dynamic laser scattering show bimodal distributions for both gibbsite and kaolinite. The gibbsite distribution indicates 80% of the population has a 0.3 μm diameter, while 20% of the population has a 1 μm diameter. The kaolinite distribution indicates 4% of the population has an average diameter of 0.3 μm, and 96% of the population has an average diameter of 4 μm (Figure 3.3 A and B).

3.2 Surface Complexation Modeling

After systematic fitting, the fit remained the same when certain reactions were removed. These reactions were not aiding the fit and were removed, keeping only reactions contributing to the final model. Additionally, it is difficult to distinguish certain surface complexes if the stoichiometry is similar, such as a monodentate and a dimer reaction.

3.2.1 Cd^{2+} on Gibbsite Modeling

Bidentate Cd^{2+} sorption on gibbsite was modeled and fitted using data from experiments G-22. The log K for the bidentate complexation reaction was the only fitted equilibrium constant. Sorption onto gibbsite is well represented by the fit, with an R^2 value of 0.99 (Figure 3.4A). Using the bidentate log K, a monodentate reaction and a dimer reaction were used to describe surface complexation on G-23, two orders of magnitude higher than experiment G-22. The monodentate reaction was determined to be unnecessary, and was not included in the final fits. Sorption onto gibbsite was described with a bidentate complex and a dimer complex with an R^2 of 0.30 (Figure 3.4B). The distribution of surface species as a function of pH can be viewed in Figure 3.4C, in which the bidentate and dimer complexes form simultaneously and plateau at pH 6. Dimer complexes represent ~25% of the total surface complexation.

3.2.2 Cd^{2+} on Kaolinite Modeling

Bidentate Cd^{2+} sorption on kaolinite was modeled and fitted using data from experiments K-25. The conditional equilibrium constant (K) for the bidentate complexation reaction was the only fitted parameter. A bidentate surface complex and a fixed deprotonation constant describe very low surface coverage sorption onto kaolinite with an R^2 of 0.99 (see Figure 3.5A). Using the fitted bidentate log K, a monodentate

reaction was fitted using data from experiment K-26. A dimer complex was also included for consideration, but was not necessary for describing the data. At two orders of magnitude higher than K-25, the K-26 uptake curve could be described by a deprotonation constant in addition bidentate, monodentate, and site-specific outer-sphere reactions with a R^2 of 0.98 (Figure 3.5B). The distribution of surface complexes (Figure 3.5C) shows that monodentate complexation is minimal, and bidentate complexation is relatively constant. Outer-sphere complexation represents ~85% of the sorbed Cd^{2+}, particularly above pH 6.

4. DISCUSSION

Although there are many surface hydroxyl sites on the kaolinite and gibbsite surfaces, only a certain fraction of surface sites are energetically available for surface complexation reactions. For this reason, there is a limit to the amount of sorbate, in this case Cd^{2+}, which may be sorbed. We postulate that at a low surface coverage, Cd^{2+} will be more likely to take up two sites to form a bidentate complex than at high surface coverage, when there is less room for sorption. At high surface coverage, fewer sites are available for interaction and may be shielded by bidentate complexes, and will become more important as the surface reaches saturation.

4.1 Cd^{2+} sorption on Gibbsite

Data from low Cd^{2+} concentration experiment G-22 is well fit by a single bidentate reaction, which is the primary surface complex at low surface coverage. There are far more available sites than can be filled when sorption of G-22 reaches 100%, which would mean that at 9.6 sites/nm^2, only 0.04% of the sites are filled. Even at higher surface coverage in G-23, only 4% of the sites are filled, but different reactions are

needed to accommodate the additional Cd^{2+}. Both bidentate and dimer complexes from simultaneously, but underestimate the amount of total sorption. From XANES linear combination fits in Chapter 2, the dimer (Cd/Al(s)) component is a large proportion of the spectral fit (50-70%) and while dimers may be forming, it is likely that there is reformation of the gibbsite surface occurring (Farley et al., 1985). Surface reformation may be an important component to gibbsite complexation behavior, and could explain additional sorption of Cd^{2+} on gibbsite that was not represented in this model.

4.2 Cd^{2+} sorption on Kaolinite

Low Cd^{2+} concentration experiment K-25 is well fit by a single bidentate reaction, which is the primary surface complex at low surface coverage. There are far more available sites than can be filled when sorption of K-25 reaches 100%, which would mean that at 1.5 sites/nm^2 only 0.6% of sites are filled. At higher surface coverage in K-26, a different dynamic must take place in order to accommodate Cd^{2+} on 57% of sites. Bidentate complexes form as sorption begins on the kaolinite surface, while there is plenty of space for bidentate surface complexes. Outer-sphere complexation dramatically increases at pH 6, and is responsible for about 85% of Cd^{2+} sorption, versus a 55% component in linear combination fits. Bidentate complexes account for about 15% of the adsorbed Cd^{2+}, while monodentate complexation only represents a very small fraction of the total. Modeling of K-26 was well represented by the bidentate log K extracted from the modeling of K-25, and the fitting of monodentate and outer-sphere reactions.

5. CONCLUSIONS

Low-coverage experiment G-22 is well represented by a deprotonation reaction and a modeled bidentate reaction. High-coverage experiment G-23 is poorly represented by fixed bidentate and fit dimer complexation reactions Surface reformation may be an important component to gibbsite complexation behavior, and could explain additional sorption of Cd^{2+} on gibbsite that was not represented in this model. Low coverage experiment K-25 is well represented by a deprotonation reaction and a modeled bidentate reaction. High coverage experiment K-26 is well represented by a fixed bidentate reaction, and modeled monodentate and outer-sphere reactions. In the high coverage kaolinite model, bidentate and outer-sphere complexation are the two most important reactions, with outer-sphere being especially important to complexation above pH 6. Cd^{2+} uptake on both gibbsite and kaolinite at low coverage can be described by bidentate complexation. At higher surface coverage, complexation is dominated by bidentate complexes (monomer and dimer) on gibbsite, and by outer-sphere complexes on kaolinite. This is consistent with what was observed in linear combination fits in Chapter 2.

6. TABLES

Table 3.1 – Stoichiometry, reactions, and constants included in the Models.

Gibbsite sorption reactions

Reaction	Log K	z0	z1	Source	Model
$\equiv AlOH_2^{0.5+} \rightarrow \equiv AlOH^{0.5-} + H^+$	-10	-0.5	0	[a]	both
$2\equiv AlOH^{0.5-} + Cd^{2+} + H_2O \rightarrow (\equiv AlOH)_2CdOH + H^+$	5.1	0.33	0.67	This study	Low surface coverage
$2\equiv AlOH^{0.5-} + 2Cd^{2+} + 3H_2O \rightarrow (\equiv AlOH)_2Cd_2(OH)_3 + 3H^+$	-0.6	0.33	0.67	This study	High surface coverage

Kaolinite sorption reactions

Reaction	Log K	z0	z1	Source	Model
$\equiv AlOH_2^{0.5+} \rightarrow \equiv AlOH^{0.5-} + H^+$	-6	-0.5	0	PZC[b]	both
$2\equiv AlOH^{0.5-} + Cd^{2+} + H_2O \rightarrow (\equiv AlOH)_2CdOH + H^+$	-2.9	0.33	0.67	This study	Low surface coverage
$\equiv AlOH^{0.5-} + Cd^{2+} + H_2O \rightarrow \equiv AlOHCdOH^{0.5+} + H^+$	-14.2	0.33	0.67	This study	High surface coverage
$\equiv AlOH^{0.5-} + Cd(H2O)_6^{2+} + H_2O \rightarrow \equiv AlOH(H_2O)_6CdOH^{0.5+} + H^+$	-4.7	0	0	This study	High surface coverage

[a](Hiemstra et al., 1989a). Point of Zero Charge (PZC) for Kaolinite is approximately 6.
[b](Dzenitis, 1997) and is used as the log K of the kaolinite deprotonation equation according to Van Riemsdijk and Hiemstra (Van Riemsdijk and Hiemstra, 2006).

Table 3.2. Mineral surface parameters and thermodynamic data for aqueous complexes

	Kaolinite (100) (Kga-2)	Gibbsite (100) (Micral 916)	Reference
Surface Area, N_2 BET (m^2/g)	17.6	22.9	This study
Site density, model (sites/nm^2)	1.5	9.6	[a, b]
Capacitances (F/m^2)	1.1, 5	1.1, 5	[c]

Aqueous Phase Reactions	Log K	Reference
$Cd^{+2} + Cl^- = CdCl^+$	1.98	wateq4f database[d]
$Cd^{+2} + 2Cl^- = CdCl_2$	2.6	"
$Cd^{+2} + 3Cl^- = CdCl_3^-$	2.4	"
$Cd^{+2} + H_2O = CdOH+ + H^+$	-10.08	"
$Cd^{+2} + 2H_2O = Cd(OH)_2 + 2H^+$	-20.35	"
$Cd^{+2} + 3H_2O = Cd(OH)_3^- + 3H^+$	-33.3	"
$Cd^{+2} + 4H_2O = Cd(OH)_4^{-2} + 4H^+$	-47.35	"
$2Cd^{+2} + H_2O = Cd2OH^{+3} + H+$	-9.39	"
$Cd^{+2} + H_2O + Cl^- = CdOHCl^+ H^+$	-7.404	"

[a](Brady et al., 1996) [b](Hiemstra et al., 1989a) [c](Hiemstra and Van Riemsdijk, 1991) [d] Updated with Powell et al. 2011

7. FIGURES

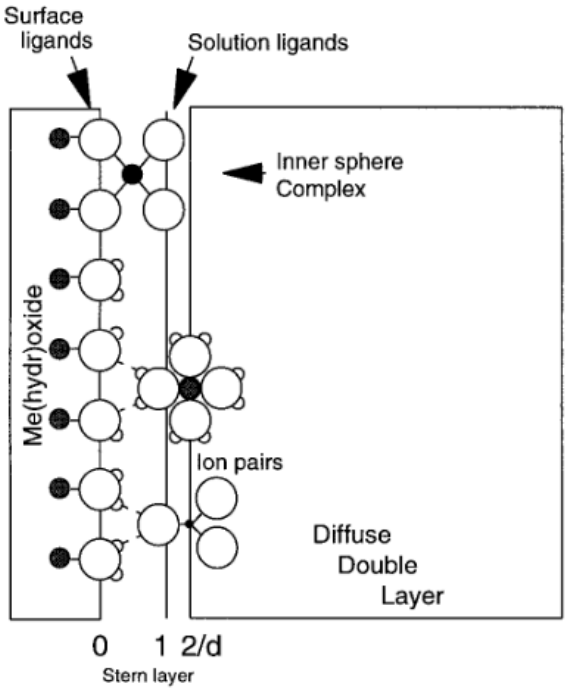

Figure 3.1

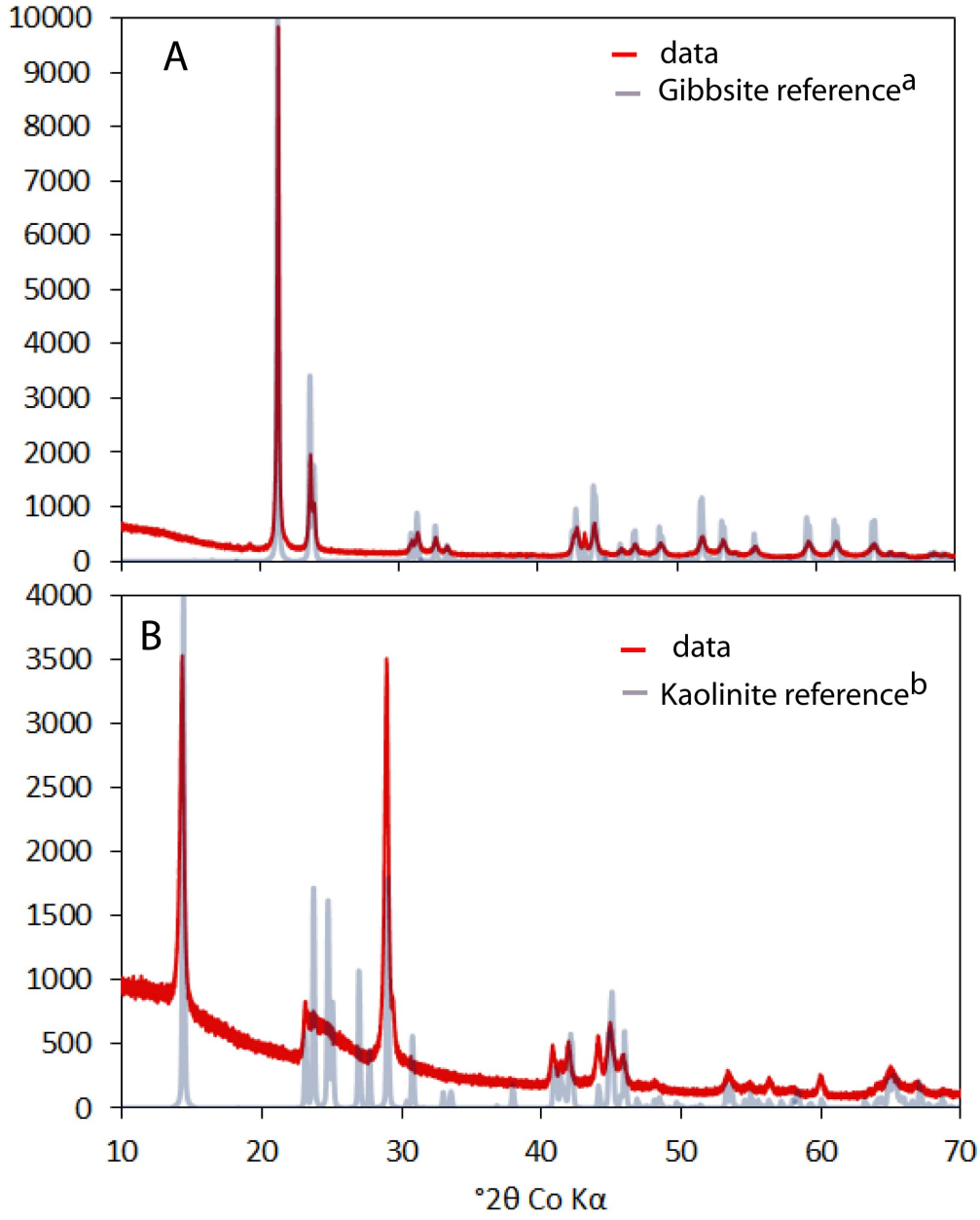
A
data
Gibbsite reference[a]
10000
9000
8000
7000
6000
5000
4000
3000
2000
1000
0
B
data
Kaolinite reference[b]
4000
3500
3000
2500
2000
1500
1000
500
0
10
20
30
40
50
60
70
°2θ Co Kα

Figure 3.2 A & B

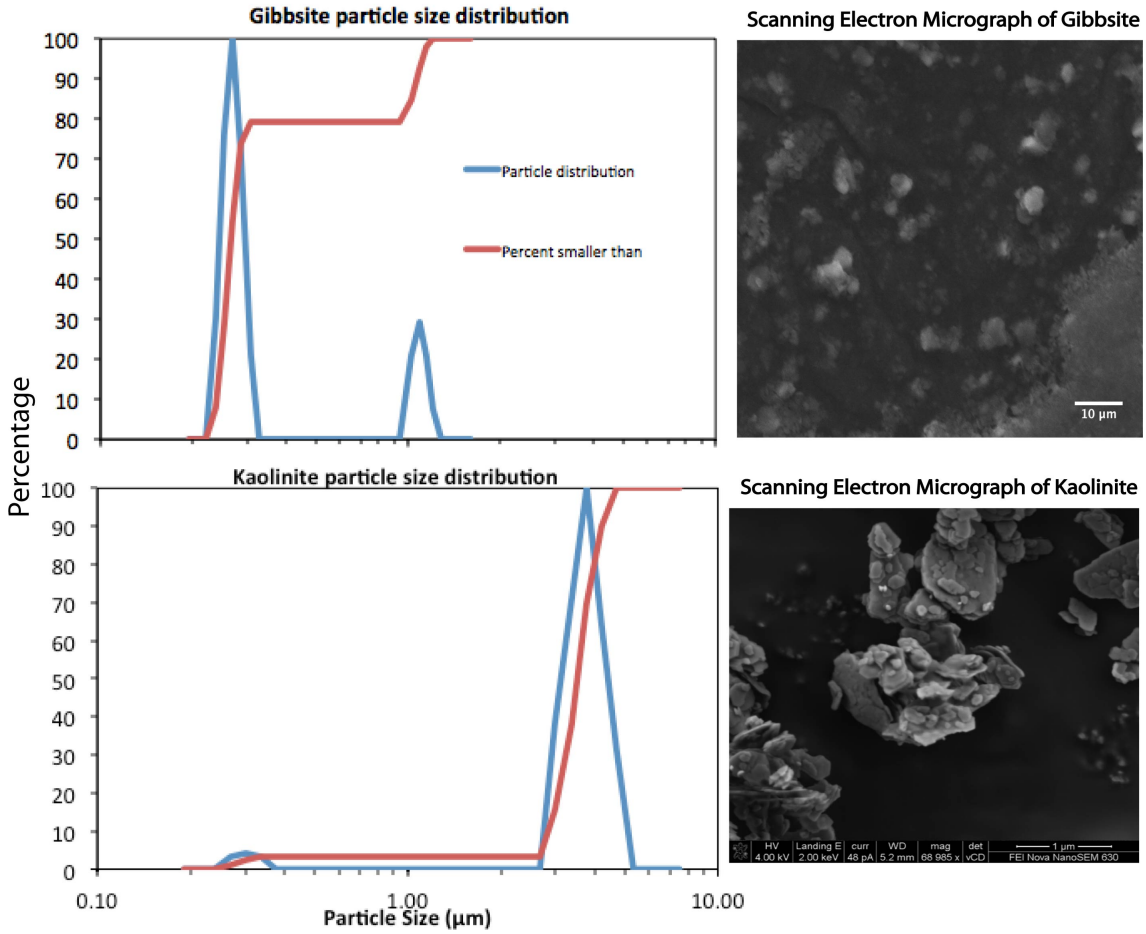
Gibbsite particle size distribution
Scanning Electron Micrograph of Gibbsite
Particle distribution
Percent smaller than
Percentage
10 µm
Kaolinite particle size distribution
Scanning Electron Micrograph of Kaolinite
0.10
1.00
10.00
Particle Size (µm)

Figure 3.3 A & B

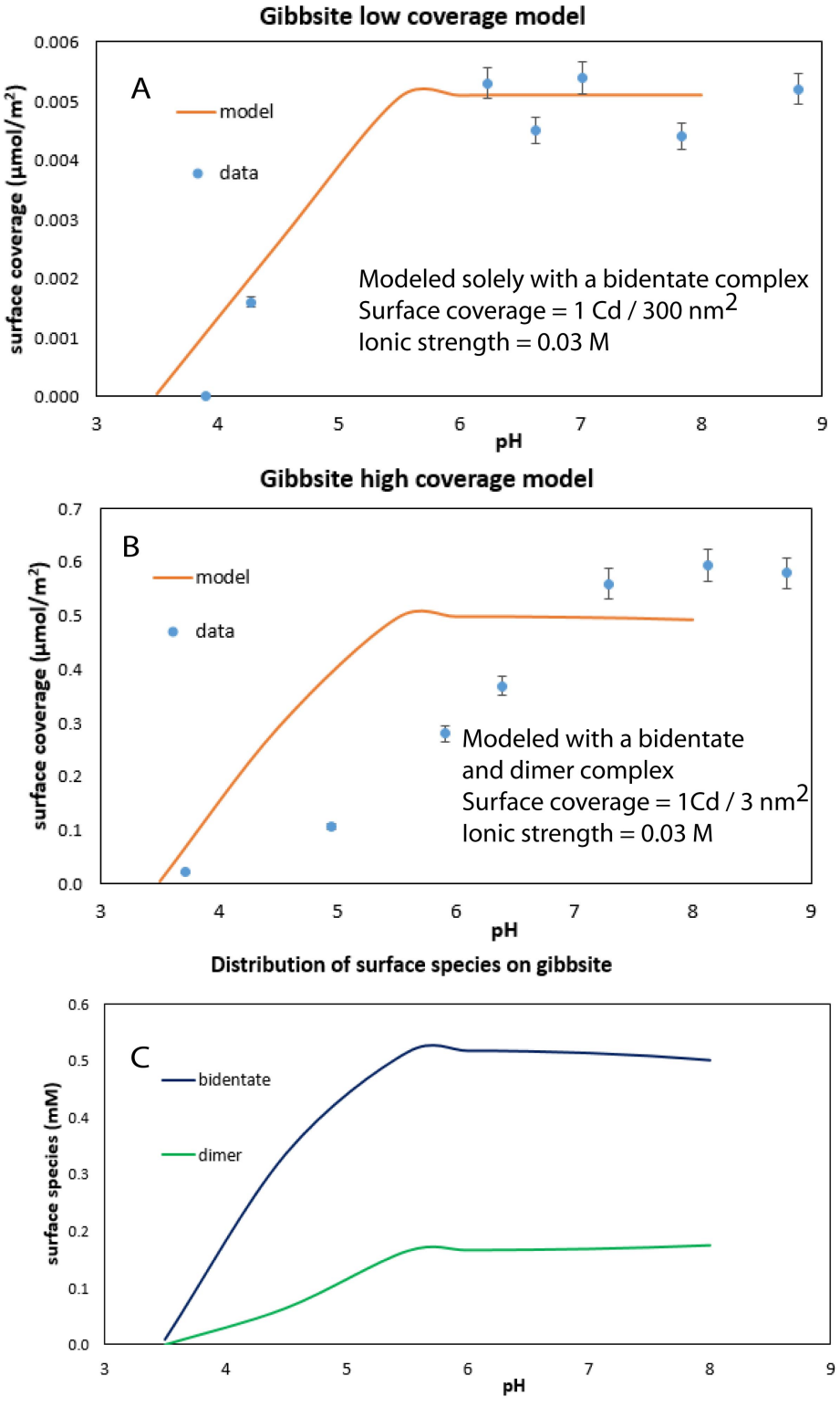
Gibbsite low coverage model
A
model
data
Modeled solely with a bidentate complex
Surface coverage = 1 Cd / 300 nm2
Ionic strength = 0.03 M
surface coverage (µmol/m2)
pH
Gibbsite high coverage model
B
model
data
Modeled with a bidentate
and dimer complex
Surface coverage = 1Cd / 3 nm2
Ionic strength = 0.03 M
surface coverage (µmol/m2)
pH
Distribution of surface species on gibbsite
C
bidentate
dimer
surface species (mM)
pH

Figure 3.4 A-C

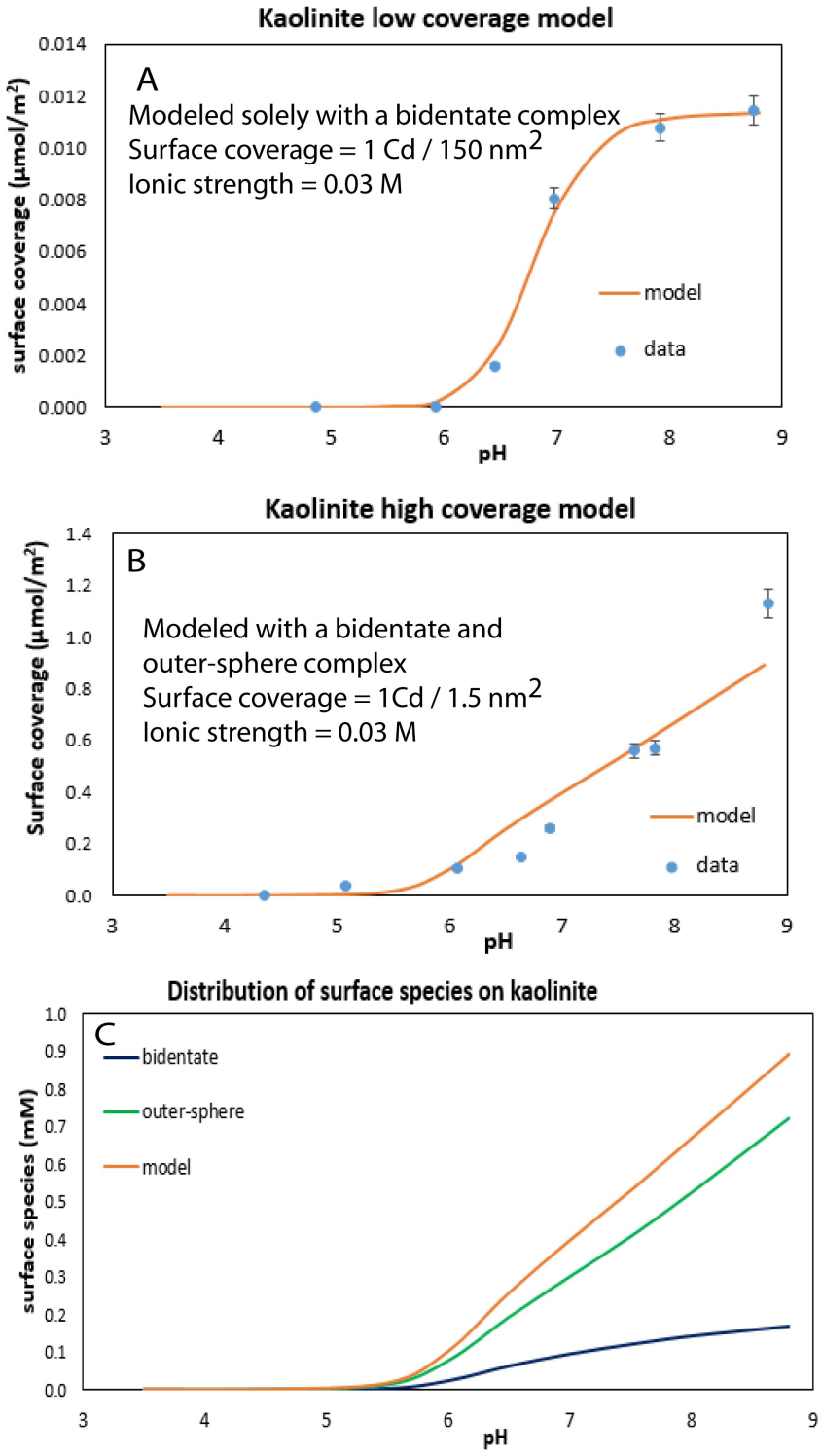
Kaolinite low coverage model
A
Modeled solely with a bidentate complex
Surface coverage = 1 Cd / 150 nm2
Ionic strength = 0.03 M
surface coverage (µmol/m2)
0.014
0.012
0.010
0.008
0.006
0.004
0.002
0.000
3
4
5
6
7
8
9
pH
model
data
Kaolinite high coverage model
B
Modeled with a bidentate and
outer-sphere complex
Surface coverage = 1Cd / 1.5 nm2
Ionic strength = 0.03 M
Surface coverage (µmol/m2)
1.4
1.2
1.0
0.8
0.6
0.4
0.2
0.0
3
4
5
6
7
8
9
pH
model
data
Distribution of surface species on kaolinite
C
bidentate
outer-sphere
model
surface species (mM)
1.0
0.9
0.8
0.7
0.6
0.5
0.4
0.3
0.2
0.1
0.0
3
4
5
6
7
8
9
pH

Figure 3.5 A-C

Figure 3.1.

Depiction of the Charge Distribution and Triple Layer Model on an oxide mineral with an inner sphere complex (top) contained within the Stern layer, and an outer sphere complex bridging the Stern layer. Figure from Figure 2 in Hiemstra and Van Riemsdijk (1996).

Figure 3.2. A & B.

A. XRD Spectra of gibbsite Micral 916 "Alumina Trihydrate" From Huber Engineered Material. [a](Saalfeld and Wedde, 1974) **B.** XRD Spectra of kaolinite KGa-2 from the Clay Minerals Society b(Bish and Von Dreele, 1989)

Figure 3.3.A & B.

A. Dynamic laser scattering results from gibbsite batch 1, with scanning electron micrograph of gibbsite. B. Dynamic laser scattering results from kaolinite batch 3, with scanning electron micrograph of kaolinite courtesy of Suzanne Estok at Pennsylvania State University.

Figure 3.4.A-C

A. Fitting of a bidentate reaction to experiment G-22. **B**. Fitting of a monodentate reaction to experiment G-23 data points with bidentate log K as a constant. **C**. Chart showing the concentrations of bidentate (blue) and dimer (orange) Cd^{2+} complexes on the gibbsite surface.

Figure 3.5. A-C

A. Fitting of a bidentate reaction to experiment K-25 data points. **B**. Fitting of a monodentate reaction to experiment K-26 data points with bidentate log K as a constant. **C**. Chart showing the concentrations of bidentate (blue) and monodentate (green) Cd^{2+} complexes on the kaolinite surface.

8. REFERENCES

A.T.S.D.R., 2008. Cadmium Toxicity: Where is Cadmium Found?, Environmental Health and Medicine Education.

Bish, D., Von Dreele, R., 1989. Rietveld refinement of non-hydrogen atomic positions in kaolinite. Clays and Clay Minerals 37, 289-296.

Farley, K.J., Dzombak, D.A., Morel, F.M., 1985. A surface precipitation model for the sorption of cations on metal oxides. Journal of Colloid and Interface Science 106, 226-242.

Gu, X., Evans, L.J., 2008. Surface Complexation modelling of Cd(II), Cu(II), Ni(II), Pb(II) and Zn(II) adsorption onto kaolinite. Geochimica Et Cosmochimica Acta 72, 267-276.

Hiemstra, T., deWit, J.C.M., Van Riemsdijk, W.H., 1989a. Multisite proton adsorption modeling at the solid/solution interface on (hydr) oxides—A new approach: II. Application to various important (hydr) oxides. Journal of Colloid and Interface Science 133, 105-117.

Hiemstra, T., Van Riemsdijk, W., 1991. Physical chemical interpretation of primary charging behaviour of metal (hydr) oxides. Colloids and surfaces 59, 7-25.

Hiemstra, T., Van Riemsdijk, W., Bolt, G., 1989. Multisite proton adsorption modeling at the solid/solution interface of (hydr) oxides: A new approach: I. Model description and evaluation of intrinsic reaction constants. Journal of colloid and interface science 133, 91-104.

Hiemstra, T., Van Riemsdijk, W.H., 1996. A surface structural approach to ion adsorption: the charge distribution (CD) model. Journal of Colloid and Interface Science 179, 488-508.

Kinniburgh, D., Cooper, D., 2011. PhreePlot: Creating graphical output with PHREEQC.

Kresse, G., Furthmüller, J., 1996. Efficient iterative schemes for ab initio total-energy calculations using a plane-wave basis set. Physical Review B 54, 11169–11186.

Kresse, G., Furthmüller, J., Hafner, J., 1994. Theory of the crystal structures of selenium and tellurium: The effect of generalized-gradient corrections to the local-density approximation. Physical Review B 50, 13181-13185.

Kresse, G., Hafner, J., 1993. Ab initio molecular dynamics for open-shell transition metals. Physical Review B 48, 13115-13118.

Kresse, G., Hafner, J., 1994. Ab initio molecular-dynamics simulation of the liquid-metal-amorphous-semiconductor transition in germanium. Physical Review B 49, 14251-14269.

Lopata, K., Van Kuiken, B.E., Khalil, M., Govind, N., 2012. Linear-response and real-time time-dependent density functional theory studies of core-level near-edge X-ray absorption. Journal of Chemical Theory and Computation 8, 3284-3292.

Machesky, M.L., Predota, M., Wesolowski, D.J., Vlcek, L., Cummings, P.T., Rosenqvist, J., Ridley, M.K., Kubicki, J.D., Bandura, A.V., Kumar, N., Sofo, J.O., 2008. Surface protonation at the rutile (110) interface: Explicit incorporation of solvation structure within the refined MUSIC model framework. Langmuir 24, 12331-12339.

Parkhurst, D.L., Appelo, C.A.J., 1999. User's guide to PHREEQC Version 2- A computer program for speciation, batch reaction, one-dimensional transport and inverse geochemical calculations, Water Resources Investigations. US Geological Survey, Lakewood, CO.

Pauling, L., 1949. A resonating-valence-bond theory of metals and intermetallic compounds. Proceedings of the Royal Society of London. Series A. Mathematical and Physical Sciences 196, 343-362.

Powell, K.J., Brown, P.L., Byrne, R.H., Gajda, T., Hefter, G., Leuz, A.-K., Sjöberg, S., Wanner, H., 2011. Chemical speciation of environmentally significant metals with inorganic ligands. Part 4: The Cd2++ OH–, Cl–, CO32–, SO42–, and PO43–systems (IUPAC Technical Report). Pure and Applied Chemistry 83, 1163-1214.

Saalfeld, H., Wedde, M., 1974. Refinement of the crystal structure of gibbsite,(AlOH) 3. Z. Krystallogr 139, 129-135.

Serrano, S., O'Day, P.A., Vlassopoulos, D., Garcia-Gonzalez, M.T., Garrido, F., 2009. A surface complexation and ion exchange model of Pb and Cd competitive sorption on natural soils. Geochimica Et Cosmochimica Acta 73, 543-558.

Sposito, G., 1984. The Surface Chemistry of Soils. Oxford University Press, New York.

Srivastava, P., Singh, B., Angove, M., 2005. Competitive adsorption behavior of heavy metals on kaolinite. Journal of Colloid and Interface Science 290, 28-38.

Stern, O., 1924. Theory of the electrical double layer.(In German.). Electrochemistry 30, 508-516.

Stumm, W., Morgan, J.J., 1996. Aquatic Chemistry: Chemical Equilibria and Rates in Natural Waters, 3 ed. John Wiley & Sons.

U.S.E.P.A., 1992. Cadmium Compounds (A), Technology Transfer Network - Air Toxics Web Site.

Valiev, M., Bylaska, E.J., Govind, N., Kowalski, K., Straatsma, T.P., Van Dam, H.J., Wang, D., Nieplocha, J., Apra, E., Windus, T.L., 2010. NWChem: a comprehensive and scalable open-source solution for large scale molecular simulations. Computer Physics Communications 181, 1477-1489.

Van Kuiken, B.E., Valiev, M., Daifuku, S.L., Bannan, C., Strader, M.L., Cho, H., Huse, N., Schoenlein, R.W., Govind, N., Khalil, M., 2013. Simulating Ru L3-Edge X-ray Absorption Spectroscopy with Time-Dependent Density Functional Theory: Model Complexes and Electron Localization in Mixed-Valence Metal Dimers. The Journal of Physical Chemistry A 117, 4444-4454.

Van Riemsdijk, W.H., Hiemstra, T., 2006. The CD-MUSIC model as a framework for interpreting ion adsorption on metal (hydr)oxide surfaces, in: Lützenkirchen, J. (Ed.), Surface Complexation Modeling. Elsevier.

Weerasooriya, R., Dharmasena, B., Aluthpatabendi, D., 2000. Copper-gibbsite interactions: an application of 1-pK surface complexation model. . Colloids and Surfaces A: Physicochemical and Engineering Aspects 170.

Yang, X., Sun, Z., Wang, D., Forsling, W., 2007. Surface acid–base properties and hydration/dehydration mechanisms of aluminum (hydr) oxides. Journal of colloid and interface science 308, 395-404.

Zhang, Z., Fenter, P., Cheng, L., Sturchio, N.C., Bedzyk, M.J., Predota, M., Bandura, A., Kubicki, J.D., Lvov, S.N., Cummings, P.T., Chialvo, A.A., Ridley, M.K., Benezeth, P., Anovitz, L., Palmer, D.A., Machesky, M.L., Wesolowski, D.J., 2004. Ion adsorption at the rutile-water interface: Linking molecular and macroscopic properties. Langmuir 20, 4954-4969.

Chapter 4: Next Steps

Future work with the Reactive Surface Area project should focus on:

1. Sensitivity analysis of Cd L_{III} XANES references by making pre-mixed standards, such as 50% $Cd(OH)_2$(s) and 50% $CdCl_2$(s), to determine with what certainty we can identify these references with linear combination fitting.
2. XANES collection of a low surface coverage Cd/gibbsite sorption sample, similar in surface coverage to IS-Kaol, to determine if IS-Kaol and low surface coverage gibbsite spectrum have similar features.
3. More study on the surface reformation properties of gibbsite at high Cd^{2+} surface coverage, perhaps with Cd K-edge EXAFS.
4. Further investigation of the Cd/Al(s) reference compound, including TEM, TGA, and perhaps Cd K-edge EXAFS.
5. Experimental interpretations would be aided by DFT calculations that involve the sequential addition of Cd2+ to the mineral surface, such as a Cd^{2+} cation added to a previously reduced bidentate model.
6. Investigation of Pb/kaolinite and Pb/gibbsite sorption samples using XANES (Perhaps Pb L3 or M1 edge?) in a similar fashion to Chapter 2, with quantitative sensitivity analysis mentioned in step one.
7. Completion of Pb surface complexation model with CD-MUSIC.
8. Surface complexation modeling of Cd/Pb competition experiments.
9. Cd^{2+} sorption experiments on goethite, which could be investigated using Cd L_{III} XANES and Fe EXAFS.

APPENDIX

TABLE A.1. Experimental conditions for Cd sorption on gibbsite

Spectrum Name (Ch.2)	Exp #	Gibbsite Batch	Initial Cd^{2+} (mM)	Initial Ca^{2+} (mM)	Initial Cl^{-} (mM)	IS (mM)	Min mass (g)	Soln Vol (ml)	Reaction time	XAS
-	G-1	1	0.05	10	20	30	0.6	10	24 h	No
-	G-2	1	0.05	100	200	300	0.6	10	24 h	No
-	G-3	1	3.7	7.4	30	37	1.2	25	24 h	No
-	G-6	2	3.5	15.5	40	58	0.49	10	24 h	No
-	G-7	2	3.5	2	13	18	0.49	10	24 h	No
-	G-8	2	3.5	0.65	10	13	0.49	10	24 h	No
-	G-9	2	3.5	15.5	40	58	0.49	10	24 h	No
G-0.41a	G-10	1	0.8	9.2	20	30	0.6	12.5	1 mo	Yes
G-1.8a	G-11	1	4	6	20	30	0.6	12.5	1 mo	Yes
-	G-12	1	0.8	9.2	20	30	0.6	12.5	2 w	No
-	G-13	1	4	6	20	30	0.6	12.5	2 w	No
-	G-14	1	0.8	9.2	20	30	0.6	12.5	1 w	No
-	G-15	1	4	6	20	30	0.6	12.5	1 w	No
-	G-16	2	0.8	0.92	3	5	0.49	12.5	24 h	No
-	G-17	1	0.8	9.2	20	30	0.6	12.5	24 h	No
G-0.42H	G-18	1	0.8	108	218	326	0.6	12.5	24 h	Yes
G-1.6L	G-19	2	4	0.6	9	14	0.49	12.5	24 h	Yes
G-1.6	G-20	1	4	6	20	30	0.6	12.5	24 h	Yes
G-1.6H	G-21	1	4	44	96	144	0.6	12.5	24 h	Yes
-	G-22	1	0.01	10	20	30	0.6	10	24 h	No
-	G-23	1	1	10	20	30	0.6	10	24 h	μprobe XAS
-	G-24	1	0.01	10	20	30	0.6	10	24 h	No
G-0.04	G-25	1	0.1	10	20	30	0.6	10	24 h	Yes
G-0.37	G-26	1	1	10	20	30	0.6	10	24 h	Yes

TABLE A.2. Experimental conditions for Cd sorption on kaolinite

Spectrum Name	Exp #	Kaolinite batch	Initial Cd^{2+} (mM)	Initial Ca^{2+} (mM)	Initial Cl^{-} (mM)	IS (mM)	Min mass (g)	Soln Vol (ml)	Reaction time	XAS
-	K-2	2	4	6	20	30	0.988	25	24 h	Yes
-	K-3	2	0.05	10	20	30	0.5	10	24 h	No
-	K-4	2	0.05	55	110	165	0.5	10	24 h	No
-	K-5	3	0.045	10	20	30	0.47	11	24 h	No
-	K-6	3	0.045	55	110	165	0.47	11	24 h	No
-	K-7	3	0	5.9	11.9	18	0.47	11	24 h	No
-	K-8	3	0.45	9.5	20	30	0.47	11	24 h	No
-	K-9	3	3.7	8.1	31	39	0.95	27	24 h	No
-	K-10	3	0.9	8.2	20	28	0.47	11	24 h	No
-	K-11	3	0.9	60	124	184	0.47	11	24 h	No
-	K-12	3	3.7	6.3	27	34	0.95	27	24 h	No
-	K-15	3	0.8	9.2	20	30	0.4	12.5	2 w	No
-	K-16	3	4	6	20	30	0.4	12.5	2 w	No
-	K-17	3	0.8	9.2	20	30	0.4	12.5	1 w	No
-	K-18	3	4	6	20	30	0.4	12.5	1 w	No
-	K-19	3	0.8	4	10	14	0.4	12.5	24 h	No
-	K-20	3	0.8	9.2	20	30	0.4	12.5	24 h	Yes
-	K-21	3	0.8	108	218	326	0.4	12.5	24 h	No
K-1.9L	K-22	3	4	4	16	24	0.4	12.5	24 h	Yes
K-1.8	K-23	3	4	6	20	30	0.4	12.5	24 h	Yes
K-1.7H	K-24	3	4	44	96	144	0.4	12.5	24 h	No
-	K-25	3	0.01	10	20	30	0.4	10	24 h	No
-	K-26	3	1	10	20	30	0.4	10	24 h	µprobe XAS
IS-Kaol	K-27	3	0.01	10	20	30	0.4	10	24 h	Yes
K-0.1	K-28	3	0.1	10	20	30	0.4	10	24 h	Yes
K-0.3	K-29	3	1	10	20	30	0.4	10	24 h	Yes

TABLE A.3. Slurries produced and used in experiments documented in the previous table.

Slurry	Mineral source	density (g/ml)	g dry/g slurry	g dry/ml slurry	SSA (m^2/g)	Suspension ($CaCl_2$)	XRD	SEM	DLS
Kaolinite1	Kga-1b	1.16	0.143	0.166	9.7±0.2	0.01	No	No	No
Kaolinite2	Kga-2	1.042	0.095	0.010	16.2±0.05	0.01	Yes	No	No
Kaolinite3	Kga-2	1.036	0.076	0.079	17.6±0.08	0.01	Yes	Yes	Yes
Gibbsite1	Micral	1.062	0.113	0.120	22.9±0.07	0.01	Yes	Yes	Yes
Gibbsite2	Micral	1.038	0.094	0.097	25.7±0.1	0.001	Yes	No	No

Table A4 Final Experimental Results for Cd sorption on Kaolinite

Thesis Expt Number	Expt Number	Initial concentration Cd (mM)	final soln conc (M)	Surface coverage	µmol/m2	pH	error (mol/m2)
K-2	Experiment 2	4.00	4.84E-04	2.47E-07	2.47E-01	6.75	2.03E-06
K-2		4.80	5.51E-04	2.74E-07	2.74E-01	6.75	2.27E-06
K-3	Experiment 3	0.05	4.48E-05	0.00E+00	0.00E+00	3.85	-1.34E-11
K-3		0.05	4.44E-05	0.00E+00	0.00E+00	4.60	-3.79E-11
K-3		0.05	4.37E-05	1.90E-09	1.90E-03	5.49	1.21E-11
K-3		0.05	3.58E-05	6.65E-09	6.65E-03	6.06	3.95E-11
K-3		0.05	2.29E-05	1.24E-08	1.24E-02	6.41	3.90E-11
K-3		0.05	9.31E-06	2.97E-08	2.97E-02	6.89	4.10E-11
K-3		0.05	3.41E-06	3.46E-08	3.46E-02	7.21	1.16E-09
K-3		0.05	1.20E-06	3.24E-08	3.24E-02	7.77	7.67E-10
K-4	Experiment 4	0.05	4.66E-05	2.43E-09	2.43E-03	3.93	1.91E-11
K-4		0.05	4.68E-05	1.08E-09	1.08E-03	4.63	3.83E-12
K-4		0.05	4.52E-05	3.12E-09	3.12E-03	5.50	1.42E-11
K-4		0.05	4.07E-05	4.92E-09	4.92E-03	6.00	4.56E-11
K-4		0.05	3.22E-05	1.36E-08	1.36E-02	6.39	1.39E-10
K-4		0.05	1.79E-05	2.72E-08	2.72E-02	6.91	3.36E-10
K-4		0.05	9.51E-06	3.23E-08	3.23E-02	7.39	5.23E-10
K-4		0.05	5.29E-06	3.42E-08	3.42E-02	7.80	3.47E-10
K-5	Experiment5	0.05	4.57E-05	0.00E+00	0.00E+00	3.93	-3.02E-11
K-5		0.05	4.67E-05	0.00E+00	0.00E+00	4.65	2.56E-13
K-5		0.05	4.66E-05	0.00E+00	0.00E+00	5.55	-5.50E-12
K-5		0.05	4.51E-05	2.77E-09	2.77E-03	6.03	2.42E-11
K-5		0.05	3.45E-05	1.16E-08	1.16E-02	6.49	1.53E-10
K-5		0.05	1.94E-05	2.65E-08	2.65E-02	6.88	1.77E-10
K-5		0.05	7.55E-06	3.75E-08	3.75E-02	7.26	5.16E-10
K-5		0.05	2.62E-06	4.36E-08	4.36E-02	7.84	5.39E-10
K-6	Experiment6	0.05	4.03E-05	2.67E-09	2.67E-03	3.90	4.31E-12
K-6		0.05	4.15E-05	6.99E-09	6.99E-03	4.66	3.63E-11
K-6		0.05	4.19E-05	2.08E-09	2.08E-03	5.58	3.84E-11
K-6		0.05	4.03E-05	5.85E-09	5.85E-03	6.07	9.78E-11
K-6		0.05	3.66E-05	1.19E-08	1.19E-02	6.45	1.07E-10
K-6		0.05	2.48E-05	2.03E-08	2.03E-02	6.84	1.66E-10
K-6		0.05	1.45E-05	3.09E-08	3.09E-02	7.25	5.63E-11
K-6		0.05	7.29E-06	3.75E-08	3.75E-02	7.81	4.45E-10
K-8	Experiment8	0.45	4.08E-04	2.70E-08	2.70E-02	3.76	1.69E-10
K-8		0.45	4.34E-04	2.45E-08	2.45E-02	4.62	1.69E-10
K-8		0.45	4.29E-04	3.69E-08	3.69E-02	5.52	4.05E-10
K-8		0.45	4.12E-04	5.46E-08	5.46E-02	5.96	5.44E-10

K-8		0.45	3.67E-04	9.60E-08	9.60E-02	6.45	5.75E-10	0.60%
K-8		0.45	3.03E-04	1.47E-07	1.47E-01	6.89	1.21E-09	0.82%
K-8		0.45	2.10E-04	2.40E-07	2.40E-01	7.31	4.65E-09	1.94%
K-8		0.45	1.07E-04	3.39E-07	3.39E-01	7.85	5.23E-09	1.55%
K-9	Experiment11	3.70	2.61E-03	1.83E-06	1.83E+00	7.81	6.92E-09	0.38%
K-9		3.70	2.61E-03	1.98E-06	1.98E+00	7.80	1.27E-08	0.64%
K-9		3.70	2.57E-03	2.02E-06	2.02E+00	7.84	3.32E-09	0.16%
K-12	Experiment18	3.70	1.88E-03	2.84E-06	2.84E+00	8.04	2.47E-08	0.87%
K-12		3.70	2.00E-03	2.54E-06	2.54E+00	8.00	1.88E-08	0.74%
K-12		3.70	2.00E-03	1.93E-06	1.93E+00	7.97	8.45E-09	0.44%
K-12		3.70	2.03E-03	2.55E-06	2.55E+00	7.91	2.56E-08	1.00%
K-14	Experiment 19	4.00	2.15E-03	3.17E-06	3.17E+00	7.53	3.02E-08	0.95%
K-16		4.00	2.10E-03	3.17E-06	3.17E+00	7.85	2.28E-08	0.72%
K-18		4.00	2.14E-03	3.18E-06	3.18E+00	7.59	2.90E-08	0.91%
K-22		4.00	2.28E-03	2.81E-06	2.81E+00	7.82	9.01E-09	0.32%
K-23		4.00	2.21E-03	3.05E-06	3.05E+00	7.78	3.54E-08	1.16%
K-24		4.00	2.24E-03	2.93E-06	2.93E+00	7.80	5.56E-09	0.19%
K-13		0.80	1.44E-04	1.10E-06	1.10E+00	7.61	1.10E-08	1.00%
K-15		0.80	3.49E-04	7.07E-07	7.07E-01	8.02	7.63E-09	1.08%
K-17		0.80	2.21E-04	8.94E-07	8.94E-01	7.80	4.42E-09	0.49%
K-19		0.80	4.05E-04	6.12E-07	6.12E-01	8.22	1.22E-08	2.00%
K-20		0.80	3.14E-04	7.76E-07	7.76E-01	7.67	1.40E-08	1.80%
K-21		0.80	3.75E-04	6.80E-07	6.80E-01	7.98	3.04E-09	0.45%
K-25	Experiment 22	0.01	9.48E-06	2.13E-09	2.13E-03	4.36	2.23E-11	1.05%
K-25		0.01	8.26E-06	1.07E-09	1.07E-03	4.87	1.43E-11	1.33%
K-25		0.01	3.56E-08	2.87E-09	2.87E-03	8.74	8.64E-11	3.01%
K-25		0.01	7.01E-06	1.51E-09	1.51E-03	6.45	7.11E-12	0.47%
K-25		0.01	8.24E-06	1.05E-09	1.05E-03	5.93	9.38E-12	0.89%
K-25		0.01	2.05E-06	2.32E-09	2.32E-03	6.98	3.97E-11	1.71%
K-25		0.01	2.14E-07	2.73E-09	2.73E-03	7.92	9.30E-11	3.40%
K-26	Experiment 23	1.00	7.84E-04	1.13E-07	1.13E-01	4.36	9.12E-10	0.80%
K-26		1.00	8.78E-04	1.45E-07	1.45E-01	5.08	3.43E-10	0.24%
K-26		1.00	8.33E-04	1.47E-07	1.47E-01	6.07	2.48E-09	1.69%
K-26		1.00	7.21E-04	1.70E-07	1.70E-01	6.89	1.38E-09	0.81%
K-26		1.00	7.94E-04	1.53E-07	1.53E-01	6.64	6.68E-10	0.44%
K-26		1.00	4.96E-04	2.13E-07	2.13E-01	7.64	1.89E-09	0.89%
K-26		1.00	9.73E-05	2.97E-07	2.97E-01	8.83	3.22E-09	1.09%
K-27	24L	0.01	0.00E+00	1.27E-08	1.27E-02	8.35	1.52E-10	1.19%
K-28	24M	0.10	1.81E-06	1.41E-07	1.41E-01	8.59	2.11E-09	1.50%
K-29	24H	1.00	5.12E-04	5.67E-07	5.67E-01	7.83	6.69E-09	1.18%

Table A5 Final Experimental Results for Cd sorption on Gibbsite

Thesis Expt Number	Expt Number	Initial concentration Cd (mM)	final soln conc (M)	Surface coverage	µmol/m2	pH	error (mol/m2)	RSD
G-1	experiment9	0.05	4.44E-05	4.96E-09	4.96E-03	4.23	5.75E-11	1.16%
G-1		0.05	2.71E-05	1.73E-08	1.73E-02	4.80	6.40E-11	0.37%
G-1		0.05	6.63E-06	3.33E-08	3.33E-02	5.67	1.04E-10	0.31%
G-1		0.05	9.99E-07	3.74E-08	3.74E-02	6.07	3.22E-10	0.86%
G-1		0.05	0.00E+00	3.82E-08	3.82E-02	6.47	1.92E-10	0.50%
G-1		0.05	0.00E+00	3.80E-08	3.80E-02	6.83	4.07E-10	1.07%
G-1		0.05	0.00E+00	3.98E-08	3.98E-02	7.36	6.39E-10	1.61%
G-1		0.05	0.00E+00	3.86E-08	3.86E-02	7.86	2.01E-09	5.20%
G-2	Experiment 10	0.05	4.43E-05	1.58E-08	1.58E-02	4.25	1.28E-10	0.81%
G-2		0.05	2.99E-05	2.20E-08	2.20E-02	4.76	2.08E-10	0.94%
G-2		0.05	9.57E-06	3.47E-08	3.47E-02	5.70	2.61E-10	0.75%
G-2		0.05	4.34E-06	4.06E-08	4.06E-02	6.11	7.61E-11	0.19%
G-2		0.05	0.00E+00	4.28E-08	4.28E-02	6.51	8.03E-10	1.88%
G-2		0.05	0.00E+00	4.50E-08	4.50E-02	6.94	7.28E-10	1.62%
G-2		0.05	0.00E+00	4.63E-08	4.63E-02	7.37	6.78E-10	1.46%
G-2		0.05	0.00E+00	3.99E-08	3.99E-02	7.82	9.13E-10	2.29%
G-3	Experiment11	3.7	1.13E-03	2.72E-06	2.72E+00	7.81	1.02E-08	0.38%
G-3		3.7	1.09E-03	2.54E-06	2.54E+00	7.80	1.79E-08	0.70%
G-3		3.7	1.04E-03	2.49E-06	2.49E+00	7.82	1.79E-08	0.72%
G-6	Experiment14	3.5	1.90E-03	5.22E-07	5.22E-01	4.23	4.99E-09	0.96%
G-6		3.5	2.02E-03	6.36E-07	6.36E-01	4.75	7.55E-09	1.19%
G-6		3.5	1.99E-03	7.97E-07	7.97E-01	5.66	7.20E-09	0.90%
G-6		3.5	1.94E-03	9.42E-07	9.42E-01	6.10	1.25E-08	1.33%
G-6		3.5	1.74E-03	1.09E-06	1.09E+00	6.50	8.62E-09	0.79%
G-6		3.5	1.36E-03	1.34E-06	1.34E+00	7.01	2.11E-08	1.58%
G-6		3.5	8.28E-04	1.69E-06	1.69E+00	7.43	1.55E-08	0.92%
G-6		3.5	4.67E-04	1.97E-06	1.97E+00	7.86	3.90E-08	1.98%
G-7	Experiment15	3.5	2.04E-03	4.03E-07	4.03E-01	4.15	1.98E-09	0.49%
G-7		3.5	2.16E-03	4.95E-07	4.95E-01	4.60	3.09E-09	0.62%
G-7		3.5	2.18E-03	6.69E-07	6.69E-01	5.54	5.23E-09	0.78%
G-7		3.5	2.03E-03	7.85E-07	7.85E-01	5.97	2.21E-09	0.28%
G-7		3.5	1.74E-03	1.00E-06	1.00E+00	6.53	5.88E-09	0.59%
G-7		3.5	1.30E-03	1.25E-06	1.25E+00	6.90	9.41E-09	0.75%
G-7		3.5	5.08E-04	1.81E-06	1.81E+00	7.47	1.48E-08	0.82%
G-7		3.5	1.55E-04	2.15E-06	2.15E+00	7.93	2.72E-08	1.27%
G-8	Experiment16	3.5	1.89E-03	3.60E-07	3.60E-01	4.05	8.43E-10	0.23%

G-8		3.5	2.18E-03	5.60E-07	5.60E-01	4.52	6.04E-10	0.11%
G-8		3.5	2.18E-03	6.87E-07	6.87E-01	5.47	3.60E-09	0.52%
G-8		3.5	1.98E-03	8.93E-07	8.93E-01	5.99	5.00E-09	0.56%
G-8		3.5	1.70E-03	1.08E-06	1.08E+00	6.36	4.85E-09	0.45%
G-8		3.5	1.16E-03	1.46E-06	1.46E+00	6.89	4.35E-09	0.30%
G-8		3.5	4.47E-04	2.04E-06	2.04E+00	7.35	1.25E-08	0.61%
G-8		3.5	5.05E-05	2.43E-06	2.43E+00	7.90	4.86E-08	2.00%
G-9	Experiment17	3.5	1.74E-03	5.24E-07	5.24E-01	4.34	8.25E-09	1.57%
G-9		3.5	1.98E-03	6.88E-07	6.88E-01	4.63	1.38E-09	0.20%
G-9		3.5	2.00E-03	8.82E-07	8.82E-01	5.47	6.99E-09	0.79%
G-9		3.5	1.93E-03	9.54E-07	9.54E-01	5.87	6.95E-09	0.73%
G-9		3.5	1.68E-03	1.18E-06	1.18E+00	6.37	4.93E-09	0.42%
G-9		3.5	1.35E-03	1.39E-06	1.39E+00	6.79	3.60E-09	0.26%
G-9		3.5	7.57E-04	1.80E-06	1.80E+00	7.25	3.36E-08	1.87%
G-9		3.5	2.31E-04	2.30E-06	2.30E+00	7.68	2.18E-08	0.95%
G-11	Experiment19	4	7.02E-04	2.90E-06	2.90E+00	7.73	1.92E-08	0.66%
G-13		4	7.89E-04	2.76E-06	2.76E+00	7.89	1.11E-08	0.40%
G-15		4	7.65E-04	2.78E-06	2.78E+00	7.79	3.61E-08	1.30%
G-19		4	9.28E-04	2.60E-06	2.60E+00	7.94	2.07E-08	0.80%
G-20		4	1.10E-03	2.63E-06	2.63E+00	7.81	1.06E-08	0.40%
G-21		4	9.05E-04	2.60E-06	2.60E+00	7.91	1.28E-08	0.49%
	Experiment 14S	3.5	1.24E-04	2.45E-06	2.45E+00	8.50	1.54E-08	0.63%
		3.5	7.95E-05	2.41E-06	2.41E+00	8.67	3.74E-08	1.55%
		3.5	1.30E-04	2.36E-06	2.36E+00	8.45	1.77E-08	0.75%
		3.5	1.63E-04	2.32E-06	2.32E+00	8.31	6.63E-09	0.29%
G-10	Experiment 19	0.8	2.46E-05	6.78E-07	6.78E-01	7.84	9.46E-09	1.40%
G-12		0.8	1.70E-05	6.82E-07	6.82E-01	8.18	7.58E-09	1.11%
G-14		0.8	1.84E-05	6.62E-07	6.62E-01	7.95	4.95E-09	0.75%
G-16		0.8	5.64E-05	6.28E-07	6.28E-01	7.92	7.75E-09	1.23%
G-17		0.8	1.30E-05	7.00E-07	7.00E-01	8.09	6.82E-09	0.98%
G-18		0.8	2.25E-05	6.54E-07	6.54E-01	7.94	5.74E-09	0.88%
G-22	Experiment 20	0.01	9.56E-06	8.32E-10	8.32E-04	3.90	9.69E-12	1.16%
G-22		0.01	5.36E-06	1.50E-09	1.50E-03	4.28	1.17E-09	0.78
G-22		0.01	3.20E-07	2.81E-09	2.81E-03	6.23	4.43E-11	1.58%
G-22		0.01	3.74E-07	2.18E-09	2.18E-03	6.63	2.70E-11	1.24%
G-22		0.01	9.79E-08	2.55E-09	2.55E-03	7.02	1.51E-09	59.02%
G-22		0.01	1.78E-08	2.06E-09	2.06E-03	7.84	1.60E-10	7.77%
G-22		0.01	0.00E+00	2.44E-09	2.44E-03	8.80	2.37E-10	9.70%
G-23	Experiment 21	1	8.39E-04	1.26E-07	1.26E-01	3.93	1.21E-09	0.96%
G-23		1	7.14E-04	1.61E-07	1.61E-01	4.88	2.05E-09	1.27%

G-23		1	5.09E-04	2.02E-07	2.02E-01	5.96	2.60E-09	1.29%
G-23		1	3.77E-04	2.26E-07	2.26E-01	6.38	3.92E-09	1.73%
G-23		1	1.05E-04	2.78E-07	2.78E-01	7.23	3.36E-09	1.21%
G-23		1	1.47E-05	2.82E-07	2.82E-01	8.09	1.15E-09	0.41%
G-23		1	4.23E-06	2.74E-07	2.74E-01	8.68	6.78E-10	0.25%
G-24	Experiment 25 L	0.01	0.00E+00	6.31E-09	6.31E-03	8.57	9.00E-10	14.27%
G-25	25M	0.1	0.00E+00	7.17E-08	7.17E-02	8.47	4.53E-09	6.32%
G-26	25H	1	2.40E-05	6.24E-07	6.24E-01	7.96	6.77E-09	1.08%

Table A6 Final Experimental Results for Pb sorption on Kaolinite

	Initial concentration Pb (mM)	final soln conc (M)	Surface coverage (mol/m2)	pH	error	RSD
Experiment 3	0.05	1.06E-06	3.31E-08	5.37E+00	2.72E-09	8.2%
Experiment 3	0.05	1.39E-07	3.60E-08	6.00E+00	1.43E-08	39.7%
Experiment4	0.05	1.56E-06	3.87E-08	5.43E+00	2.38E-09	6.2%
Experiment4	0.05	1.65E-07	3.93E-08	5.90E+00	2.04E-08	51.9%
Experiment5	0.045	3.84E-06	4.05E-08	5.43E+00	1.92E-09	4.7%
Experiment5	0.045	3.33E-07	4.41E-08	6.05E+00	2.25E-08	51.1%
Experiment6	0.045	5.47E-06	3.86E-08	5.46E+00	6.35E-10	1.6%
Experiment6	0.045	1.15E-06	4.73E-08	6.02E+00	9.78E-09	20.7%
Experiment7	0.045	2.34E-06	3.53E-08	5.41E+00	1.33E-09	3.8%
Experiment7	0.045	3.72E-07	3.80E-08	5.98E+00	2.22E-08	58.5%
Experiment 11	3.7	3.12E-03	1.09E-06	5.40E+00	7.97E-09	0.7%
Experiment 11	3.7	3.22E-03	1.11E-06	5.46E+00	1.07E-09	0.1%
Experiment 11	3.7	3.14E-03	1.29E-06	5.41E+00	2.16E-08	1.7%
Experiment18	3.7	2.98E-03	7.92E-07	5.32E+00	8.23E-09	1.0%
Experiment18	3.7	2.93E-03	8.43E-07	5.37E+00	1.43E-08	1.7%
Experiment18	3.7	2.92E-03	8.24E-07	5.42E+00	1.33E-09	0.2%
Experiment18	3.7	2.87E-03	9.24E-07	5.43E+00	4.22E-09	0.5%

Table A7 Final Experimental Results for Pb sorption on Gibbsite

	Initial concentration Pb (mM)	final soln conc (M)	Surface coverage (mol/m2)	pH	error	RSD
Experiment9	0.05	8.29E-07	3.77E-08	5.43E+00	1.58E-08	41.9%
Experiment9	0.05	1.97E-07	3.82E-08	5.93E+00	2.24E-08	58.7%
Experiment10	0.05	4.69E-06	3.65E-08	5.32E+00	4.04E-10	1.1%
Experiment10	0.05	8.69E-07	3.89E-08	6.02E+00	7.13E-09	18.3%
Experiment11	3.7	3.13E-03	6.44E-07	5.43E+00	7.28E-09	1.1%
Experiment11	3.7	2.98E-03	6.91E-07	5.44E+00	1.00E-08	1.5%
Experiment11	3.7	3.21E-03	6.77E-07	5.44E+00	4.01E-09	0.6%
Experiment14	1	4.56E-04	3.21E-07	5.55E+00	2.46E-09	0.8%
Experiment14	1	1.92E-04	5.60E-07	6.07E+00	8.10E-09	1.4%
Experiment15	1	6.18E-04	2.31E-07	5.43E+00	2.97E-09	1.3%
Experiment15	1	2.75E-04	5.27E-07	6.09E+00	3.98E-09	0.8%
Experiment16	1	6.24E-04	2.28E-07	5.56E+00	2.04E-09	0.9%
Experiment16	1	3.37E-04	4.68E-07	6.01E+00	5.18E-09	1.1%
Experiment17	1	4.58E-04	3.39E-07	5.53E+00	4.95E-09	1.5%
Experiment17	1	1.79E-04	5.96E-07	6.11E+00	3.87E-09	0.6%